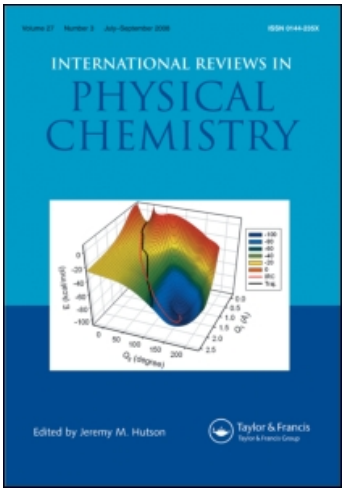

International Reviews in Physical Chemistry
Publication details, including instructions for authors and subscription information:
http://www.informaworld.com/smpp/title~content=t713724383

Reactions of mass-selected cluster ions in a thermal bath gas

A. A. Viggiano; Susan T. Arnold; Robert A. Morris

Online publication date: 26 November 2010

To cite this Article Viggiano, A. A. , Arnold, Susan T. and Morris, Robert A.(1998) 'Reactions of mass-selected cluster ions in a thermal bath gas', International Reviews in Physical Chemistry, 17: 2, 147 — 184
To link to this Article: DOI: 10.1080/014423598230126
URL: http://dx.doi.org/10.1080/014423598230126

INTERNATIONAL REVIEWS IN PHYSICAL CHEMISTRY, 1998, VOL. 17, NO. 2, 147–184

Reactions of mass-selected cluster ions in a thermal bath gas

by A. A. VIGGIANO, SUSAN T. ARNOLD and ROBERT A. MORRIS

Air Force Research Laboratory, Space Vehicles Directorate, Battlespace Environment Division (VSBP), 29 Randolph Road, Hanscom Air Force Base, MA 01731-3010, USA

Technological developments of fast-flow tubes that led to major advances in the study of cluster ion reactions are reviewed, including the coupling of high-pressure cluster ion sources to flowing-afterglow and selected-ion flow tube (SIFT) instruments. Several areas of cluster ion chemistry that have been studied recently in our laboratory, using a SIFT instrument with a supersonic expansion ion source, are reviewed. Firstly the thermal destruction of cluster ions is highlighted by a discussion of the competition between electron detachment and thermal dissociation in hydrated electron clusters $(H_2O)_n^-$. Rates and activation energies for the thermal destruction (dissociation plus detachment) of these clusters are discussed. The reactivity of hydrated electron clusters with several neutral electron scavengers is also reviewed. Secondly cluster ion chemistry related to trace neutral detection of atmospheric species using chemical ionization mass spectrometry is discussed. Recent rate measurements needed for chemical ionization detection of SO_2 and H_2SO_4 using $CO_3^-(H_2O)_n$ ions are reviewed. Thirdly the effects of solvation on nucleophilic displacement (S_N2) reactions are highlighted by the reactions of CH_3Br with $OH^-(H_2O)_n$, $Cl^-(H_2O)_n$ and $F^-(H_2O)_n$. Our measurements show that rates of S_N2 reactions decrease with increasing hydration, and the reactions preferentially lead to unhydrated products, corroborating previous experimental and theoretical studies. The cluster studies also demonstrate that, in the absence of a fast S_N2 reaction channel, other mechanisms such as association and ligand switching can become important. In the reaction of $Cl^-(H_2O)_n$ with CH_3Br, a reaction where ligand switching plays an important role, the interesting thermal dissociation of $Cl^-(CH_3Br)$ product ions is discussed. Finally, the use of cluster reactivity studies to resolve issues about the detailed nature of solvation, that is whether the core ion is internally or externally solvated, is discussed. Size-dependent rate constants for the reactions of $X^-(H_2O)_n$ (X = F, Cl, Br or I) with Cl_2 and the reactions of $OH^-(H_2O)_n$ with CO_2 and with HBr were used to determine the closing of initial solvation shells.

1. Introduction

Cluster ion chemistry has grown into a large and varied field encompassing many disciplines. A comprehensive overview of the field has been provided by Castleman and Bowen [1]. The study of cluster ion reaction kinetics essentially began with the development of flowing-afterglow instruments. Graul and Squires [2] provide a review of flow tube technology up to 1988. Many advances have been made since that time, allowing new aspects of cluster ion chemistry to be examined in detail. This review focuses, in particular, on the study of mass-selected cluster ion reactions in a thermal bath gas. The discussion focuses on several areas of cluster chemistry that have been studied recently in our laboratory, including

(1) hydrated electron cluster reactivity and thermal dissociation processes,
(2) cluster chemistry related to trace neutral detection of atmospheric species using chemical ionization mass spectrometry,

0144–235X/98 $12.00

(3) solvation effects on nucleophilic substitution reactions and
(4) size-dependent cluster kinetics as a probe of cluster structure.

In order to put the present measurements in perspective, the remainder of the introduction is devoted to a history of cluster studies in fast-flow apparatuses, outlining the technological developments which led to major advances in the field of cluster chemistry.

Development of the flowing-afterglow technique was a major advance in the ability to study ion–molecule reactions of all types including association reactions and reactions of cluster ions. The first such instrument employed for the study of ion–molecule reactions was that of the National Oceanic and Atmospheric Administration (NOAA) group in Boulder [3]. The basic flowing-afterglow instrument consists of a flow tube (typically 7–8 cm in diameter and 1 m in length), an upstream ion source, a downstream quadrupole mass spectrometer and reagent inlets. Reactant ions are created in the upstream end of the flow tube and carried downstream by the buffer where they encounter neutral reactant molecules. Reactant ions and the resulting product ions are then sampled by the mass spectrometer. A key advantage of the flowing-afterglow instrument over other systems was that it had a well controlled reaction zone in which the formation process for the reactant ion was complete before reactant neutrals were introduced. This allowed for firstly knowledge of the reactant ion state, secondly a constant-temperature bath with no applied electric fields and thirdly the ability to vary the pressure at a known temperature. A review of the NOAA design has been provided by Ferguson *et al.* [4].

The first studies of ion clustering using a flowing-afterglow instrument were made by Ferguson and co-workers [5, 6]. These pioneering papers included reactions of metal ions associating with O_2, for example

$$Mg^+ + O_2 + Ar \rightarrow MgO_2^+ + Ar, \tag{1}$$

as well as the observation of saturation effects in three-body association reactions. A year later this same group dramatically expanded the number of association reactions and reactions involving clusters that had been studied at the time with most of the effort going into understanding the ion chemistry of the upper atmosphere. The studies involved not only new systems but also the ability to vary the temperature and pressure as well as to examine reactions of negative ions [7–10]. While at present this all may seem routine, at the time these were major advances. One study of special importance was the deduction of a reaction scheme to explain the observation of proton hydrates as the dominant ions in the mesosphere [10, 11]. The first important discovery to explain the mesospheric proton hydrates was the observation that $O_2^+(H_2O)$ reacts with H_2O to produce H_3O^+ core ions:

$$\begin{aligned} O_2^+(H_2O) + H_2O &\rightarrow H_3O^+ + OH + O_2 \\ &\rightarrow H_3O^+(OH) + O_2. \end{aligned} \tag{2}$$

Reaction (2) and the simultaneous discovery of a similar reaction involving $NO^+(H_2O)_n$ conversion to proton hydrates [12] showed that cluster ion chemistry could be not only interesting but an important natural phenomenon as well.

In the next few years, a number of groups studied many reactions involving clusters using a flowing-afterglow apparatus. Notable among these was the work done by

Kaufmann and co-workers [13–15] on reactions pertaining to the rate of formation of proton hydrates in the upper atmosphere. Another important set of studies was performed by Bohme and co-workers on the effects of solvation on nucleophilic displacement reactions and other reactions. Much of this work has been summarized in a review article [16]. During the 1970s the number of flowing-afterglow instruments in the world increased, and a list of all the reactions measured by this technique up to 1977 has been given in a compilation by Albritton [17].

A major advance in the ability to study the chemistry of ion–molecule reactions in flow tubes was made by Adams and Smith [18] with the introduction of the selected-ion flow tube (SIFT) apparatus in the mid-1970s. In this technique, the ion source is separated from the flow tube, and only one ion is mass selected and injected into the flow tube at a time. This makes measurements of kinetics very simple since only three primary species exist in the flow tube:

(1) an inert buffer in concentrations of about 10^{16} molecules cm^{-3},
(2) a reactant neutral with concentrations in the range 10^{10}–10^{14} molecules cm^{-3} and
(3) an ionic species at a concentration of approximately 1–10^{5} molecules cm^{-3}.

For cluster ions, one must worry about ligand detachment upon injection which causes more than one ion to be present in the flow tube, but the situation is still rather simple. This situation allows product ions to be easily distinguished unless they happen to have the same mass as the primary ion. Thus, both rate constants and product branching ratios can be measured readily. The external ion source not only makes the kinetics simple but also allows for ions that otherwise could not be studied in the presence of the precursor gas, for example CH_2^+. A review of many of the early studies of association reactions and reactions involving clusters performed in SIFTs has been given by Adams and Smith [19].

A few examples of these early studies are given here. Key reactions in the conversion of O_2^+ and NO^+ to proton hydrates in the upper atmosphere that could not be studied easily in the flowing afterglow were of the type

$$NO^+ + N_2 + M \rightarrow NO^+(N_2) + M, \tag{3}$$

followed by

$$NO^+(N_2) + CO_2 \rightarrow NO^+(CO_2) + N_2, \tag{4}$$

followed by

$$NO^+(CO_2) + H_2O \rightarrow NO^+(H_2O) + CO_2. \tag{5}$$

While reaction (2) and its NO^+ equivalent helped to explain the presence of proton hydrates in the mesosphere, they could not explain the rapidity of the reaction sequence due to the slow clustering of H_2O to O_2^+ and NO^+ and the small ambient H_2O concentration. Although the N_2 rate constant for association to ions is small, the large abundance of N_2 makes the overall rate rapid. The ligand switching reactions are fast, resulting in a considerable increase in the formation rate of $NO^+(H_2O)$ compared with the direct clustering. However, the bond strength of the $NO^+(N_2)$ cluster is quite weak and therefore difficult to study. While several attempts were made to study this reaction in other apparatuses, accurate rate constants were determined only with the advent of the SIFT and the use of a scavenger gas such as H_2O to make the measurements [20]. In this technique an amount of H_2O is added such that no direct clustering takes place, but a fast ligand switching to the more stable $NO^+(H_2O)$ occurs.

Other early SIFT studies involved association of hydrocarbon ions to a variety of neutrals [21]. These studies were aimed at understanding the chemistry of interstellar clouds. Examples include the reactions of CH_3^+ with a large number of neutrals including CO, O_2, N_2 and CO_2, for example

$$CH_3^+ + CO + HE \rightarrow CH_3^+(CO) + He. \quad (6)$$

Association reactions such as this are related to radiative association reactions for which the rates could be deduced from the three-body rates [22]. Many of these studies have been reviewed thoroughly elsewhere [23, 24]. An important aspect of these studies involved measuring the temperature dependences and comparing them with theory. For small systems it was found that the temperature dependence was approximately T^{-n}, where n represents the number of rotational degrees of freedom in the reactants [25, 26]. For larger systems, vibrations must also be taken into account [27].

The early SIFT instrument allowed many aspects of reactivity to be studied, but the study of reactions of cluster ions with large numbers of ligands was not possible, at least partially because clusters with many ligands could not be made in conventional ion sources. As a way around this limitation, Fahey *et al.* [28] designed a high-pressure ion source inside a flowing-afterglow instrument. This was the first modification of a flowing afterglow made explicitly to study cluster ions. It consisted of an ion source region separated from the main flow tube by a membrane. Ionization took place in the high-pressure region (tens of torr) by electron impact. This allowed clustering to take place at high pressures and generally kept the concentration of the source of the clustering agent at sufficiently small levels in the flow tube so as not to affect reactivity severely. Key to the success of this technique was the ability to cool the flow tube. The NOAA group primarily performed two sets of experiments with this source, namely the reactions of $O_2^-(H_2O)_n$ with a number of atmospheric neutrals [28] and the reactions of proton hydrates with N_2O_5 [29].

Although this technique saw limited use in its original laboratory, it has since been developed further. We used this technique in our laboratory for the first time in 1987 [30]. In that study we examined how neutral reactions proceeded when one of the neutrals was clustered to an alkali core ion, building on previous work done in the NOAA laboratory in a conventional flowing afterglow [31]. As an example, we found that the reaction

$$Li^+(NO_2) + CO \rightarrow Li^+(CO_2) + NO \quad (7)$$

is 30 orders of magnitude faster than the equivalent neutral reaction, that is $NO_2 + CO \rightarrow CO_2 + NO$. Other neutral reactions that are accelerated by clustering to alkali ions are the reactions of HBr with O, H_2S with O, N_2O with O, N_2O_5 with NO, and O_3 with NO.

One key limitation to the study of large cluster ions with the high-pressure source in a flowing afterglow is the fact that many neutrals freeze at the temperatures where cluster ions become thermally stable. In order to circumvent this problem, our laboratory improved on the basic NOAA design by adding a heated inlet [32]. This allowed for relatively large clusters, up to 11 H_2O ligands, to be studied with a variety of polar neutrals that otherwise would have frozen in the inlet, for example CH_3OH, CH_3CN, CH_3COCH_3 and C_3H_5N. Indeed the lowest temperature that could be used was determined by the freezing of the reactant neutral in the inlet. We also used this

design to study the reactions of $H^+(NH_3)_n(H_2O)_m(n+m \leqslant 5)$ with pyridine and picoline [33]. These reactions are all important in the ion chemistry of the stratosphere and/or troposphere [34], and for the first time relevant rate constants for all clusters important to atmospheric chemistry were measured. However, this design could only occasionally give detailed information on the product neutrals. Generally the family of the product ions could be identified and possibly the main product, but information on the cluster distribution in the products could not be derived accurately.

The full potential of this design has been exploited by Yang and Castleman [35, 36]. They refined the basic technique described above and were able to study clusters with up to 59 H_2O ligands. The main improvements that led to this success were improvements in the design of the heated inlet and the use of a mass spectrometer with a much larger mass range. Castleman's group [37] has produced OH^-, O^-, O_2^-, H_3O^+, HO_2^-, O_3^-, NO_2^- and NO_3^- core ions clustered to large numbers of water ligands.

The fast-flow high-pressure ion source technique has produced some very useful results on the kinetics of large cluster ions, but the information on product ions was limited in nature. For that reason, several years ago we added a supersonic expansion ion source to our variable-temperature SIFT instrument. This technique has proven to be a substantial improvement in studying both the rate constants and the products of larger cluster ions. With it we are able to produce ions heretofore unavailable for study in a thermal energy buffer gas, most notably hydrated electrons, and the technique allowed us to examine reaction products in considerable detail. In this paper, we review all the results taken to date with this source, emphasizing those results which could not have been determined using any of the past designs.

2. Experimental details

The measurements were made using a variable-temperature SIFT shown in figure 1. SIFT instruments have been the subject of numerous reviews [2, 19, 23], and therefore only the parts of the apparatus necessary for the study of mass-selected cluster ions will be discussed in detail. The most important modification necessary to study large mass-selected cluster ions in a SIFT was to replace the standard electron impact ion source with a differentially pumped source chamber housing a supersonic expansion ion source. The second important modification is the use of a heated inlet for low-temperature studies of reactant species of low vapour pressure. The use of low temperatures is important since many weakly bonded cluster ions dissociate readily at warmer temperatures. (Note that 'warmer' in this case can mean greater than 120 K.)

The supersonic expansion ion source employed here is similar in design to those used by Haberland *et al.* [38] and by Bowen and co-workers [39] which are capable of producing intense beams of large cluster ions. A high-pressure gas is expanded through a pinhole aperture into high vacuum. Typically, the stagnation chamber, which can be heated or cooled, contains a source gas or mixture at several atmospheres which is expanded through a 25 μm orifice. A biased hot filament (ThO_2/Ir) placed just downstream of the orifice ionizes the expanding jet. The bias voltage ranges from 10 V to a few hundred volts. The clusters are produced either from the primary electrons or from secondary electrons produced by collisions between primary electrons and the expansion gas. The secondary electrons have a lower energy and are presumably the prime agents of electron attachment for species such as hydrated electrons. An axial magnetic field is used to confine the electrons and to increase ion intensities. A neutral gas inlet in the expansion region allows additional gases to be

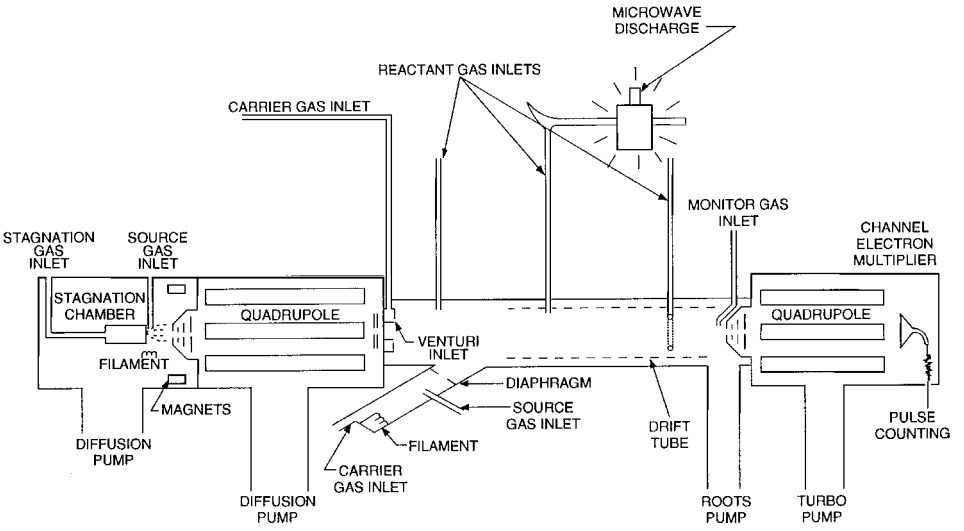

Figure 1. A schematic diagram of the modified SIFT apparatus [42]. The previous electron impact ion source has been replaced with a differentially pumped source chamber housing a supersonic expansion ion source. Cluster ions produced in the source region are sampled by a blunt skimmer and passed into the upstream quadrupole mass filter.

entrained in the expansion to allow conversion to the ion of choice. For this reason, we refer to this inlet as the entrainment inlet. This will be described in more detail later in this section.

Cluster ions produced in the source region are sampled by a blunt skimmer generally biased at a few volts with respect to the stagnation chamber. The ions are then focused by a set of ion lenses into a quadrupole mass filter. The mass-selected ions are then injected into the flow tube via a Venturi inlet and transported by a fast flow (about 7×10^3 cm s^{-1}) of buffer gas. Either helium or hydrogen are used as the buffer gas. Helium is the standard buffer gas in a SIFT; however, hydrogen is often utilized in our laboratory to minimize break-up of the weakly bonded cluster ions upon injection into the flow tube. The reason for this is straightforward; for a given injection energy in the laboratory frame, the ion-buffer centre-of-mass energy is a factor of approximately two smaller for the lighter hydrogen buffer. The difference between the helium and hydrogen buffers can be dramatic, and for many weakly bonded clusters it can be the difference between being able to detect the ion downstream and not. The bulk of the gas in this fast-flow apparatus is pumped by a Roots-type pump. Typically, the pressure is 0.1–0.2 Torr for a hydrogen buffer and 0.3–0.5 Torr for a helium buffer. The difference has to do with the differing diffusion losses in the two buffers. The buffer gas can be purified by passing it through a molecular sieve trap cooled by liquid nitrogen. This was particularly important for studies involving hydrated electrons which react with small amounts of O_2 and CO_2 in the buffer. The residence time of the ions in the flow tube was 3–20 ms as measured by time-of-flight techniques.

The flow tube is terminated by a blunt sampling cone. The primary ions and the product ions are sampled through a 0.2 mm orifice in a flat plate mounted on the blunt sampling cone (see figure 1) and mass analysed in a second quadrupole mass spectrometer. The flat plate is electrically isolated, allowing the total ion current to be monitored. This provides important data, especially when thermal electron detachment experiments are performed. In order to minimize the break-up of clusters

during sampling, we apply only about 2.5 V bias on the sampling orifice and less than 25 V bias on the next electrode. Based on our analysis of the kinetics data, these settings allowed the clusters to be sampled with less than 5% break-up [40]. This small amount of dissociation does not affect our ability to determine rate constants; however, it may have a small effect on the branching ratio determinations for minor products, although within our stated uncertainty.

The entire flow tube, from injector to sampling cone, can be heated or cooled. The stainless steel flow tube is surrounded by a copper heat exchanger in which cooling coils and heating elements are embedded. Cooling is accomplished by pulsing liquid nitrogen into the cooling coils, and heating is performed resistively. The copper heat sink distributes the heat uniformly as monitored by six resistance temperature detectors (RTDs).

Within the flow tube, there are a number of neutral gas inlets. Just downstream of the Venturi inlet, there is an inlet occasionally used for changing the identity of the primary ion or for adding a scavenger gas. Further downstream are two inlets used for introducing neutral reagents into the flow tube. By monitoring the ion signals as the flow of the reactant neutral is varied, rate constants and branching ratios can be derived using either inlet. The rate constant k is determined from

$$k = \frac{1}{\tau[\mathrm{B}]} \ln\left(\frac{A_0^{\pm}}{A^{\pm}}\right), \tag{8}$$

where τ is the reaction time, [B] is the reactant neutral concentration, $A_0^{\pm}$ is the reactant ion signal with no neutral in the flow tube and $A^{\pm}$ is the reactant ion signal at the neutral concentration [B]. The reaction time is measured by applying a pulsed retarding potential at two positions in the reaction zone. The neutral concentrations are measured by monitoring the temperature and pressure in the flow tube and the flow rates of the buffer and reactant gases.

Uncertainty in the absolute rate constants is estimated as 25%, and the uncertainty in the relative rate constants is 15% [41]. Product branching fractions were calculated without a mass discrimination correction; the correction is minimized by taking data under low-resolution conditions. The branching fractions are accurate to 5–10 percentage units as determined by reactant and product ion balance.

For studying neutral reactants with high vapour pressures, the inlets are simple 'finger inlets', $\frac{1}{8}$ inch stainless steel tubing which enters the flow tube perpendicular to the buffer flow and terminates at the radial centre of the flow tube with an elbow directing the added gas in the upstream direction. In order to study low-vapour-pressure neutral reactants, the inlet must be heated. Normally this is accomplished as follows: a thin $\frac{1}{8}$ inch stainless steel inlet line is silver soldered to a thicker $\frac{1}{4}$ inch tube, and an electrical current is passed between the two tubes. This primarily heats the thin inlet while leaving the outer tube at approximately the same temperature as the buffer gas; therefore, little warming of the buffer gas occurs. For studying sulphuric acid reactions, a more elaborate heated inlet was required. A $\frac{1}{4}$ inch glass tube was blown such that a small bulbed section, stuffed with glass wool and about 1 ml of H_2SO_4, resided just inside the inlet flange of the flow tube. The glass was wrapped with insulated Nichrome wire in two zones, one around the bulb containing H_2SO_4 and one on the straight piece of glass tubing downstream from the bulb. A RTD monitored the temperature in each of the two zones. To avoid significantly heating the buffer gas, the inlet was wrapped with thermal insulation. The insulation was then covered with

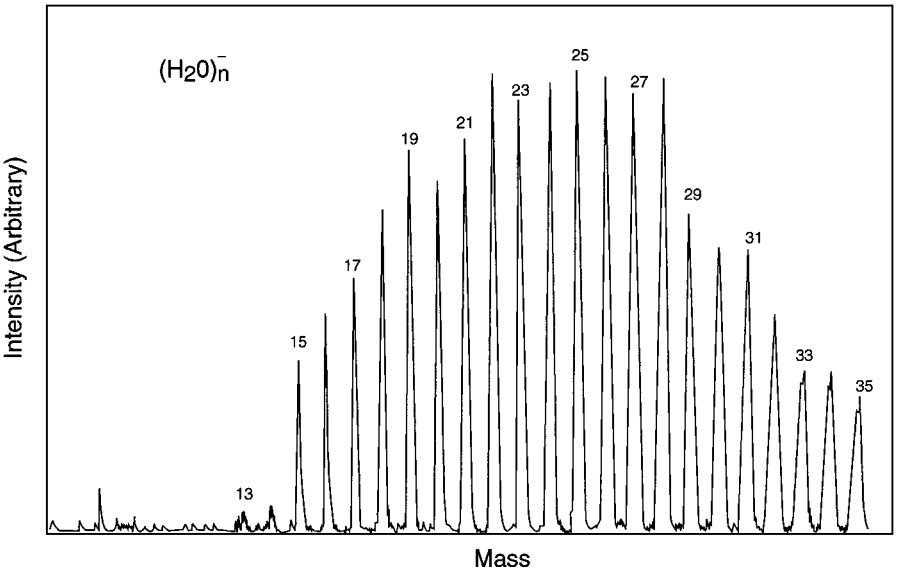

Figure 2. The distribution of hydrated electron clusters which are stable in the SIFT at 100 K are clusters in the size regime $n \geqslant 13$ [42]. At these temperatures, the source is also capable of producing clusters larger than our mass spectrometer can detect, that is greater than 700 amu.

stainless steel foil, so that no electrically insulating surface was exposed to the ions. (Insulating surfaces charge in the unipolar environment of a selected ion flow tube and cause disruption of the ion signal.) Typically, both zones of the inlet were maintained at about 373 K, and a helium carrier gas was used to carry H_2SO_4 vapour into the flow tube. Absolute concentrations of H_2SO_4 could not be determined; only relative rate constants could be measured by varying the helium carrier gas.

To date we have studied mainly negative ions containing H_2O ligands. In every case, the expansion consisted of a H_2O–Ar mixture. In such an expansion the primary negative ions are hydrated electrons $(H_2O)_n^-$ and $OH^-(H_2O)_n$ ions. The former are produced from attachment of low-energy secondary electrons to $(H_2O)_n$ clusters and the latter by high-energy electrons. Using this technique, we can make essentially any size cluster. Figure 2 shows a distribution of hydrated electrons formed this way. The mass spectrum is taken with the dc component off in the upstream quadrupole and the flow tube at 100 K. In this spectrum, one can see all clusters from $n = 15$ to the upper end of the mass range of the downstream mass spectrometer. The spectrum begins at $n = 15$ for reasons that will be explained in the results section.

The $(H_2O)_n^-$ and $OH^-(H_2O)_n$ primary ions are the precursor ions for producing other clusters. To form halide–water clusters, a reagent gas was added to the entrainment inlet. The following gases were used: NF_3 for $F^-(H_2O)_n$, CH_3Cl or CF_2Cl_2 for $Cl^-(H_2O)_n$, CH_3Br for $Br^-(H_2O)_n$, and CF_3I for $I^-(H_2O)_n$. Addition of these gases resulted in almost pure beams (greater than 90%) of the series of interest. $NO_3^-(H_2O)_n$ and $NO_3^-(HNO_3)_n$ ions were made by adding HNO_3 to the entrainment inlet. $CO_3^-(H_2O)_n$ ions were the only species that we found could not be produced by this method. Addition of CO_2 to the entrainment inlet resulted in $HCO_3^-(H_2O)_n$ ions from $OH^-(H_2O)_n$, and $CO_2^-(H_2O)_n$ ions from $(H_2O)_n^-$. To make $CO_3^-(H_2O)_n$ we added N_2O to the entrainment inlet, which resulted in $OH^-(H_2O)_n$ and $O^-(H_2O)_n$ ions. These

were injected into the flow tube and CO_2 was added in the upstream inlet, producing $CO_3^-(H_2O)_n$ and $HCO_3^-(H_2O)_n$ ions. The resolution in the upstream quadrupole was not high enough to separate the two ion series and still to have reasonable signal intensities.

We have just begun working with cation clusters. An expansion of Ar–H_2O produces $H^+(H_2O)_n$ ions in the absence of contamination. After cleaning the ion source, we have found CH_3OH and CH_3COCH_3 incorporated into the clusters, and the ease with which the contaminants have been incorporated leads us to believe that many series of cation clusters can be made.

While the goal is to work with one ion at a time, this is possible only when the cluster ions are relatively strongly bonded (greater than 15–20 kcal mol^{-1}). Dissociation of the clusters occurs both by break-up during injection and by thermal dissociation. The latter determines the upper temperature range at which measurements are possible for a particular cluster. In practice we work in several ways. Since having more than one primary ion present in the flow tube rarely interferes with the kinetic measurements, the upstream quadrupole can be set to pass a number of clusters by either turning down the resolution or turning off the dc component of the quadrupole voltage. For measuring product branching ratios, it is important to have as narrow a distribution of primary ions in the flow tube as possible. This is accomplished in several ways; we demonstrate using $Cl^-(H_2O)_n$ clusters as an example [41]. To study the reactions of $Cl^-(D_2O)$ (D_2O was used to avoid mass coincidences with $OH^-(H_2O)_2$), we injected $Cl^-(D_2O)$ into the flow tube and obtained signals of about 50–90% purity, the remainder being Cl^- due to dissociation. A smaller amount of dissociation was observed at lower temperatures. To study $Cl^-(D_2O)_n$ with $n \geqslant 2$, we used three techniques, all of which produced the same experimental results:

(1) We injected $Cl^-(D_2O)_n$ and obtained about 20% $Cl^-(D_2O)_n$ and 80% $Cl^-(D_2O)_{n-1}$.
(2) We injected $Cl^-(D_2O)_{n+1}$ at a higher injection energy chosen to dissociate one of the solvent molecules upon injection. This allowed the ion of interest to be nearly 80% of the total ion current at low temperatures, while smaller amounts were obtained at higher temperatures.
(3) We injected a broad distribution of large clusters by turning the dc off in the upstream quadrupole and setting that quadrupole to allow only $Cl^-(D_2O)_{n>4}$ ions to be injected. The flow tube temperature was then set so that all clusters larger than the desired cluster thermally decomposed in the upstream portion of the flow tube. At room temperature this resulted in about 15% $Cl^-(D_2O)_2$ and 85% $Cl^-(D_2O)$. At 233 K, this resulted in 97% $Cl^-(D_2O)_2$, 2% $Cl^-(D_2O)$ and less than 1% $Cl^-(D_2O)_3$. At 200 K, the resulting distribution was 55% $Cl^-(D_2O)_3$ and 45% $Cl^-(D_2O)_2$ with a negligible amount of $Cl^-(D_2O)$.

The last technique gave the largest signals since many clusters in the primary distribution compressed into one or two main peaks. Only the reactions of the cluster with the largest value of n and reasonable signal intensity were studied using this method. In all cases (except $CO_3^-(H_2O)_n$) we have been able to set the conditions so that only one or two main primary ions and another one or two minor primaries were present in the flow tube.

Much of the success of the technique is due to the ability to control the flow tube temperature over its entire length. Even a small warm spot often leads to thermal dissociation of the ions in the flow tube. We have used the temperature variability to

study the thermal decomposition of hydrated electrons and to determine when product ions are thermally stable by examining unusual temperature dependences of the product branching ratios.

The thermal destruction measurements of the hydrated electrons were made by injecting a narrow distribution of cluster sizes into the flow tube and then monitoring both the total ion signal and the mass-selected product ion signals as the flow tube was slowly heated from 100 K to 150 K [42]. This was done for two different distributions: one for cluster sizes near the threshold region ($14 \leqslant n \leqslant 17$) and one for large cluster sizes ($20 \leqslant n \leqslant 24$). The total ion current reaching the flat plate on the sampling cone was also recorded as a function of temperature for both distributions. The resolution of the downstream quadrupole was set to avoid mass discrimination problems, while still completely separating adjacent-sized water cluster anions. Both dissociation of a water ligand and electron detachment were observed.

The second-order rate constant for the temperature-dependent cluster destruction can be expressed in an Arrhenius form:

$$k_2 = \frac{1}{[\mathrm{H_2}]\tau} \ln\left(\frac{I_0}{I}\right) = A \exp\left(\frac{-E_\mathrm{A}}{k_\mathrm{B} T}\right), \tag{9}$$

where I_0 is the initial cluster ion intensity at 100 K, I is the temperature-dependent intensity, τ is the residence time in the flow tube, $[\mathrm{H_2}]$ is the buffer gas concentration, A is a pre-exponential factor and E_A is the activation energy associated with the destruction. For the smaller clusters in each set, some error may be introduced from the dissociation of the next larger cluster. However, this effect should be small for the above cluster sizes owing to the nature of the distribution, and this is evidenced by the smooth nature of the data as presented later.

3. Results and discussion

We have studied a number of systems using this technique. They are best discussed grouped into several categories, and this section is organized to reflect that. We start first with a discussion of hydrated electron chemistry and dissociation. The chemistry involved is rather simple and a good place to start. The discussion of the thermal dissociation processes helps one to understand the importance of thermal dissociation in determining the product distributions in other systems. Following is a discussion of chemistry related to trace neutral detection of atmospheric species using chemical ionization mass spectrometry (CIMS). A section on the effect of solvation on nucleophilic substitution follows. The results in this section clearly extend previous work on this important area and show the importance of studying these effects in an apparatus such as ours, that is we have found several problems associated with having the solvent present in the flow tube. Finally, we conclude with a section which indicates that cluster reactivity may help to resolve issues about the detailed nature of solvation, that is whether the core ion is internally or externally solvated.

3.1. *Hydrated electron clusters*

Mass spectra of hydrated electron clusters $(\mathrm{H_2O})_n^-$ generally display a continuous distribution of cluster ions beginning at $n \approx 10$–15, and occasionally, several smaller magic number species are also observed [38, 43]. Figure 2 demonstrates the cluster sizes that are observed in the SIFT apparatus at 100 K. The intensity of clusters in the threshold range $10 \leqslant n \leqslant 14$ increases when the flow tube is further cooled to 90 K.

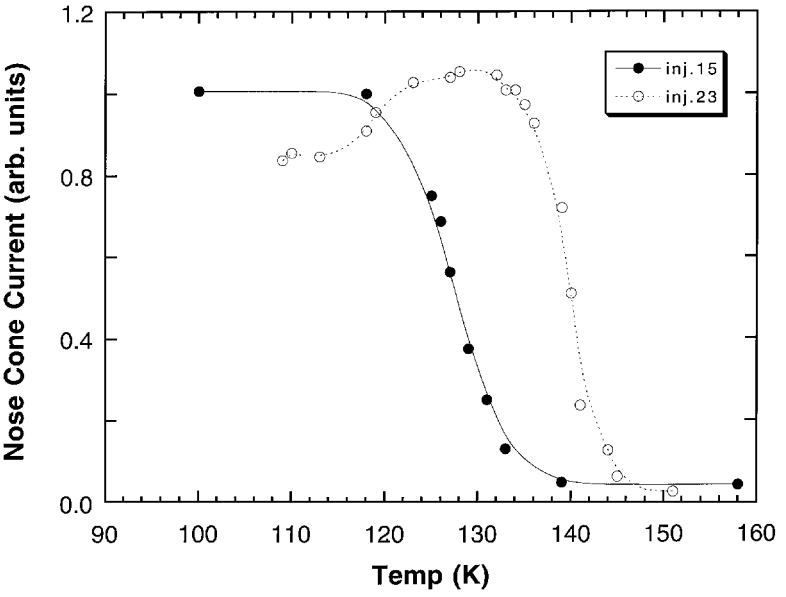

Figure 3. The total ion current measured at the sampling plate, plotted as a function of temperature [42]: (●), distribution of near-threshold-sized hydrated electron cluster ions; (○) distribution of larger clusters. In both cases, the dramatic decrease in total ion current is attributed to the ions undergoing thermal electron detachment.

The smaller clusters are not observed at 100 K because they are unstable in the buffer gas even at these low temperatures. It is believed the distribution observed in the hydrated electron mass spectra primarily results from a competition between two cluster decay channels, evaporative cooling and electron detachment:

$$(H_2O)_n^- \rightarrow (H_2O)_{n-1}^- + H_2O, \tag{10}$$

$$(H_2O)_n^- \rightarrow (H_2O)_n + e^-. \tag{11}$$

We have examined the competition between these two channels for $(H_2O)_n^-$, $14 \leqslant n \leqslant 24$, over the temperature range 100–150 K and obtained rates and activation energies for the size-dependent thermal destruction (dissociation plus detachment) of these hydrated electron clusters [42].

The complete thermal destruction of hydrated electron clusters $(H_2O)_n^-$, $14 \leqslant n \leqslant 24$, occurs in the SIFT apparatus over a narrow temperature range from 120 to 145 K. For two different distributions of clusters initially injected into the flow tube, the total ion current as measured at the flat sampling plate decreases abruptly over a narrow temperature range, as shown in figure 3. The decreasing ion current is attributed to the fact that cluster ions decay by electron detachment. (The plate current decreases when detachment occurs because free electrons diffuse much more rapidly than ions and are therefore lost very quickly to the flow tube walls.) Electron detachment occurs in the region from 120 to 130 K for a distribution of hydrated electron clusters, $13 \leqslant n \leqslant 17$, while detachment occurs at higher temperatures, 133–144 K, for a distribution of larger clusters, $20 \leqslant n \leqslant 24$, because detachment is a multistep process.

The size- and temperature-dependent competition between reactions (10) and (11) was further examined by monitoring the intensity of each cluster size as the temperature was slowly increased. Thermal destruction of the smaller cluster ions

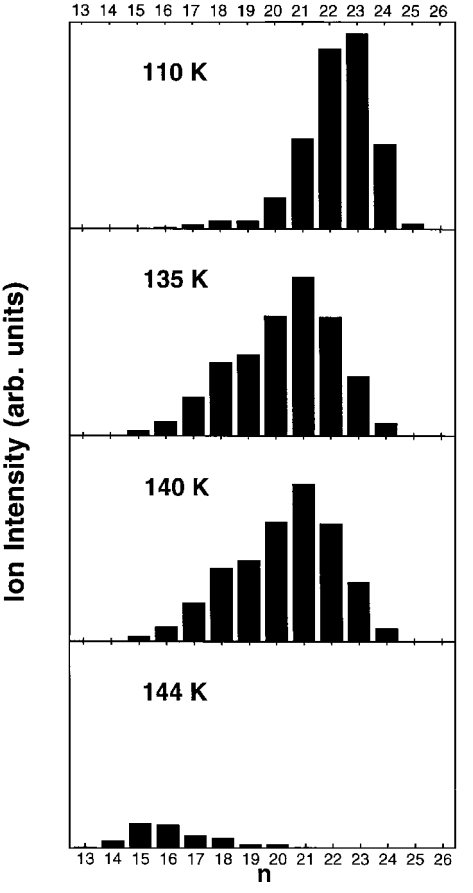

Figure 4. The initial distribution of hydrated electron clusters, $20 \leqslant n \leqslant 24$, changed significantly as the temperature was increased from 110 to 135 K, 140 K and 144 K. Initially, the ions are destroyed by evaporating water monomers. At higher temperatures, the remaining smaller cluster anions decayed by electron detachment [42].

($n < 16$) is dominated by electron detachment, as evidenced by the drop in total ion signal level with increasing temperature while the position of the cluster distribution remains relatively constant, that is no smaller hydrated electron clusters appear in the mass spectra. The destruction of larger-sized clusters ($20 \leqslant n \leqslant 24$) is illustrated in figure 4, where representations of the cluster distribution are shown at several temperatures. Initially, the clusters dissociate by the sequential evaporation of neutral water molecules, leaving behind a broadened distribution of smaller clusters without any measurable change in the total ion intensity. As the temperature increases, the electron detachment channel begins to compete with monomer evaporation. Virtually all hydrated electron clusters detach the excess electron by 145 K. Detachment occurs at higher temperatures for larger clusters because the destruction is the multistep process

$$(H_2O)_n^- \rightarrow (H_2O)_{n-1}^- \rightarrow \ldots \rightarrow (H_2O)_{n-m} + e^- , \qquad (12)$$

and only the smaller clusters detach.

Rate expressions and activation energies for the thermal destruction of hydrated electron clusters were obtained by modelling the temperature-dependent decreases in

Table 1. Activation energies E_A, second-order rate constants k_2 and pseudo-first-order rate constants k_1 for the destruction of hydrated electron clusters $(H_2O)_n^-$, $14 \leqslant n \leqslant 17$ and $23 \leqslant n \leqslant 24$. The values for k_1 and k_2 are related by the H_2 buffer gas concentration.

n	E_a (eV)	$k_2(T)$ ($cm^3\ s^{-1}$)	$k_1(T)$ (s^{-1})
14	0.06	$1.5\times10^{-12}\exp(-700/T)$	$1.2\times10^{4}\exp(-700/T)$
15	0.17	$3.2\times10^{-8}\exp(-2000/T)$	$2.6\times10^{8}\exp(-2000/T)$
16	0.26	$1.0\times10^{-4}\exp(-3000/T)$	$8.0\times10^{11}\exp(-3000/T)$
17	0.28	$5.3\times10^{-4}\exp(-3300/T)$	$4.2\times10^{12}\exp(-3300/T)$
23	0.34	$1.2\times10^{-1}\exp(-4000/T)$	$9.6\times10^{14}\exp(-4000/T)$
24	0.34	$1.2\times10^{-1}\exp(-4000/T)$	$9.6\times10^{14}\exp(-4000/T)$

the ion signals for $14 \leqslant n \leqslant 17$ and $23 \leqslant n \leqslant 24$ to an Arrhenius form (see equation (9)). The results are listed in table 1. The activation energy for thermal destruction initially increases with increasing cluster size. However, the activation energies for clusters with $n \geqslant 17$ are nearly constant at about 0.34 eV. The evaporative cooling model of Klots [44] predicts that the energy required to evaporate a single water molecule from clusters of this size is about 0.4 eV. The measured activation energies are slightly smaller. This is expected for thermal dissociation reactions in the low-pressure limit, assuming that there is no barrier in the reverse association reaction. The principle is that the activation energy is defined as the average energy of reacting molecules minus the average energy of reactants. In the low-pressure limit, the average energy of reacting molecules is just above the critical energy for reacting, that is significantly smaller than this same energy for a Boltzman distribution. In the high-pressure limit, we would find the activation energy approximately equal to the bond dissociation energy. Because the operative mechanism for thermal destruction of the smaller clusters is electron detachment, the measured activation energies can be used to further estimate the cluster's adiabatic electron affinity EA_a. We assume that $EA_a = E_A + 0.06$ eV. The estimated EA_a values for $n = 14$ and $n = 15$ are 0.12 eV and 0.23 eV respectively, values which are in reasonable agreement with those predicted by the dielectric continuum model of Barnett *et al.* [45, 46].

The present results on the thermal destruction of hydrated electron clusters are in agreement with the observations of Johnson and co-workers [47, 48] who investigated the photoinitiated and condensation-induced destruction of these clusters. These workers noted that electron detachment begins to compete with fragmentation and evaporation in the range of $n \approx 15$, which led them to speculate that the electron affinity of clusters with $n < 15$ is below the water monomer evaporation energy.

The reactions of hydrated electron clusters $(H_2O)_n^-$ with several neutral electron scavengers were studied in the SIFT apparatus at 100 K [49]. Bimolecular rate constants were determined for $(H_2O)_n^-$, $13 \leqslant n \leqslant 33$, reacting with CO_2, NO, N_2O and O_2. The products of the CO_2, NO and O_2 reactions are solvated change transfer product ions and neutral water molecules:

$$CO_2 + (H_2O)_n^- \rightarrow CO_2^-(H_2O)_{n-m} + mH_2O,\ \langle m \rangle = 1.3, \tag{13}$$

$$NO + (H_2O)_n^- \rightarrow NO^-(H_2O)_{n-m} + mH_2O,\ \langle m \rangle = 3.5, \tag{14}$$

$$O_2 + (H_2O)_n^- \rightarrow O_2^-(H_2O)_{n-m} + mH_2O,\ \langle m \rangle = 5.0. \tag{15}$$

Generally, one or two main product ions are observed for each cluster reaction, differing only in the number of water molecules solvating the charge transfer product.

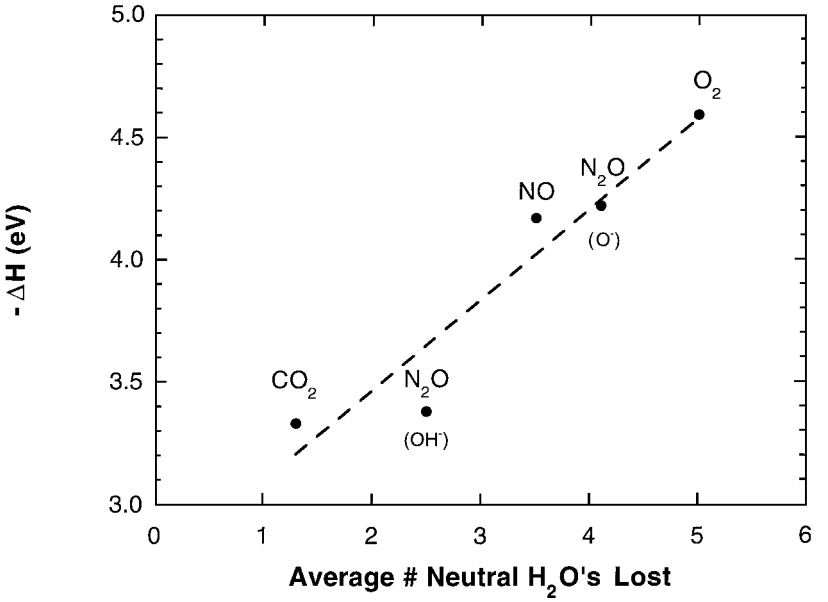

Figure 5. Plot of the overall reaction exothermicity $-\Delta H$ against the average number of neutral water molecules lost in the reaction of $(H_2O)_n^-$ with CO_2, NO, N_2O and O_2 [49]. The reaction with N_2O produces two distinct product ion distributions which are associated with different $\langle m \rangle$. The slope represents the energy required to eject a single water monomer from the cluster ions, $D[(H_2O)_n \ldots (H_2O)] \approx 0.37$ eV.

The average number $\langle m \rangle$ of water molecules lost from the cluster varies between the reaction systems as indicated in reactions (13)–(15). The reaction of $(H_2O)_n^-$ with N_2O produces two distinct dissociative charge-transfer product ion distributions:

$$\begin{aligned} N_2O + (H_2O)_n^- &\rightarrow O^-(H_2O)_{n-m} + N_2 + mH_2O, \langle m \rangle = 4.1, \\ &\rightarrow OH^-(H_2O)_{n-m} + N_2 + OH + (m-1)H_2O, \langle m \rangle = 3.5. \end{aligned} \quad (16)$$

The product branching fractions are 75% $O^-(H_2O)_{n-m}$ clusters and 25% $OH^-(H_2O)_{n-m}$ clusters. The two product channels are associated with slightly different average water monomer losses. No solvated charge transfer product ions $N_2O^-(H_2O)_n$ were observed. Further characterization of the ionic products of reactions (13)–(16) by photoelectron spectroscopy confirms that the product ion charge distribution has fundamentally changed from that of $(H_2O)_n^-$ to that of a solvated molecular anion complex $X^-(H_2O)_n$.

The number of neutral water molecules lost from the hydrated electron clusters via reaction with electron scavengers is strongly correlated to the overall reaction exothermicity [50]. For the reactions of $(H_2O)_n^-$ with CO_2, NO, N_2O and O_2, exothermicities were estimated by calculating ΔH for the following individual processes: electron detachment from the hydrated electron clusters, electron attachment to the neutral scavenger molecules, and stepwise solvation of the resulting molecular anions. The estimated ΔH_{rxn} for reactions (13)–(16) are plotted in figure 5 as functions of $\langle m \rangle$. A linear least-squares fit to the data implies that about 0.37 eV is required to eject each water monomer from the cluster, which is close to the value of about 0.4 eV calculated using the evaporative cooling model of Klots [44] and the value of 0.34 eV obtained from the SIFT thermal destruction experiments [42].

Unlike the solution-phase reactions, which proceed at or near the diffusion-controlled limit, the rates for gas-phase cluster reactions are generally lower than the corresponding collision rate. For each electron scavenger, we found that the reaction rates with hydrated electron clusters do not vary with cluster size. On average, the CO_2 reactions proceed at the collision rate, while the average NO, N_2O and O_2 reaction efficiencies are significantly smaller (80%, 63% and 35% respectively.) The cluster reaction efficiencies can be rationalized largely by spin considerations. Because some spin-allowed product species will be energetically inaccessible, the observed rate constant should be compared with the collisional rate constant multiplied by a fractional statistical weight f which is applicable to the allowed product species [51]. The expected rate constants for production of ground-state products for CO_2, NO and O_2 reactions are k_c, $\frac{3}{4}k_c$ and $\frac{1}{3}k_c$ respectively, demonstrating a general correlation between the measured rates and the rates expected from spin considerations. The inefficiency of the N_2O reactions is not explained in this manner. Other factors governing the dissociative charge transfer, including possible steric effects, may account for the fact that the observed reaction rates are only $\frac{2}{5}k_c$.

The primary force driving the evaporative charge transfer reactions can be understood on the basis of the changes in the physical dimensions of the excess electron in the reactants and the products and by a consideration of the associated Born solvation energies. Because the excess electron in $(H_2O)_n^-$ is delocalized and has a small solvation energy compared with the product solute anions, there is a critical distance as the scavenger approaches the cluster, where the excess charge is stabilized more by residing with the solute anion rather than with the water cluster. This represents a crossing in the diabatic free-energy curves and, at this point, the electron distribution can 'pour' into the electron-accepting orbital of the scavenger. The water molecules participate in the reaction by following the changing charge density.

A comparison of the present results with a previous molecular beam reactivity study [50] illustrates the competition between two cluster cooling mechanisms. In general, the molecular beam reactions, which are kinetically controlled, lose an average of 1.5–2 more water molecules compared with the flow tube reactions, where the nascent product distributions are affected by collisional cooling. The difference in water monomer loss is partly attributed to the evaporative cooling rate being significantly smaller than the collisional quenching rate and partly due to differing initial cluster temperatures with each effect accounting for about one additional H_2O lost in the beam experiment.

3.2. *Ions used as chemical ionization agents in the atmosphere*

Clusters are important in atmospheric ion chemistry [34]. Not only are all ions in the lower atmosphere solvated, but also cluster ions are important for chemical ionization detection for atmospheric trace species [52]. The ion chemistry of the natural atmosphere is essentially a solved problem [34], but the rate constants needed for chemical ionization detection of trace neutrals is still an open field. Both our group and Frank Arnold's group at the Max Planck Institut in Heidelberg use $CO_3^-(H_2O)_n$ as chemical ionization agents for measuring a variety of neutrals including SO_2, H_2SO_4, HNO_2 and HNO_3 [53–58]. We have recently measured the reactions of $CO_3^-(H_2O)_n$ with SO_2 and H_2SO_4 as well as other ions used as chemical ionization agents to detect H_2SO_4 [59, 60]. Unfortunately, because of the difficulties described earlier in making a clean source of $CO_3^-(H_2O)_n$ ions, it was not possible to determine the products for these systems.

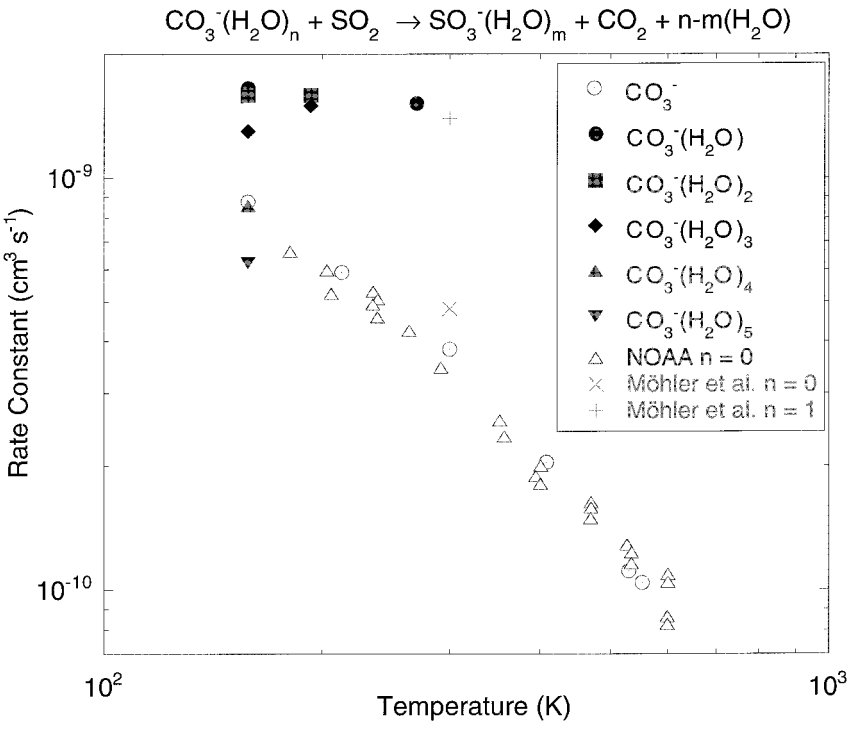

Figure 6. Rate constants for the reactions of $CO_3^-(H_2O)_n$ with SO_2 against temperature [60]. Also included are the data of Albritton *et al.* [61] and Möhler *et al.* [62].

The rate constants for the reaction of $CO_3^-(H_2O)_n$, $0 \leqslant n \leqslant 5$, with SO_2 are shown in figure 6. The coldest temperature that we could work with was 158 K, and this was also the only temperature at which $n = 4$ and $n = 5$ could be studied. At warmer temperatures, these clusters thermally dissociated and, at much colder temperatures, we had trouble introducing SO_2 into the flow tube without freezing. The $n = 0$ rate constant was observed to decrease with increasing temperature, and the data are well fitted by the power-law expression 3.52×10^{-10} $(T/300)^{-1.73}$ cm^3 s^{-1}. Our values are in excellent agreement with the values obtained by Albritton *et al.* [61]. Our room-temperature result is 20% lower than the room-temperature result of Möhler *et al.* [62], which is within the combined error limits of the measurements. The $n = 0$ reaction is exothermic by 196 kJ mol^{-1} [63, 64] but, unlike many ion–molecule reactions which proceed at the collision rate when exothermic, the $n = 0$ reaction proceeds at only a fraction of the collision rate. However, this behaviour is common with CO_3^- reactions involving O^- transfer (e.g. $CO_3^- + NO$ and $CO_3^- + NO_2$) [65].

Adding a single water molecule to CO_3^- causes the rate constant to increase by a factor of approximately two. When the temperature is raised from 158 to 270 K, the rate constant decreases by 8%, essentially temperature invariant. The rate constant is in good agreement with the value of 1.4×10^{-9} cm^3 s^{-1} reported by Möhler *et al.* [62] for $n = 1$ at 300 K. The $n = 2$ rate constant is the same as the $n = 1$ rate constant and was found to be temperature invariant from 158 to 193 K. The $n = 3$ rate constant was found to be slightly smaller than the $n = 2$ rate constant, and it displayed a slight negative temperature dependence. Unfortunately, the narrow temperature range where measurements could be made prevented an accurate assessment of the

temperature dependence. The $n = 4$ and $n = 5$ rate constants were substantially smaller than those for the $n \leqslant 3$ reactions. No previous measurements of the rate constants for $n \geqslant 2$ have been made. The decrease in the rate constant for $n = 4$ coincides with a solvation shell closing, that is all three oxygen atoms in CO_3^- have a H_2O ligand attached.

Absolute rate constants could not be measured for the H_2SO_4 reactions. Instead relative rate constants were determined by monitoring two or more reactants either simultaneously or in quick succession. Table 2 lists, among other parameters, the relative rate constants for the reactions studied here at five different temperatures, where the rate constants are relative to a different ion at each temperature. At 300 K, the only cluster ion that could be studied was $HCO_3^-(H_2O)$, and the rate constants are measured relative to the rate constant for bare CO_3^-. At 273 K, the rate constants are relative to that for NO_3^- which in turn is assumed to be the same relative rate constant as found at 300 K. At 233 K, the rate constants are relative to that of bare CO_3^-. The 200 K rate constants are relative to that of $NO_3^-(H_2O)$ which was assumed to be the same as that found at higher temperatures. Finally, at 158 K the rate constants are relative to that of $NO_3^-(HNO_3)$ which is assumed to be the average of the relative rate constants found at higher temperatures. In all cases, the relative rate constants are close to unity, ranging from 0.69 to 1.1 of that for CO_3^-.

For the most part, the relative rate constants were found to be independent of temperature. However, for $NO_3^-(HNO_3)_2$ and $NO_3^-(HNO_3)_3$ the rate constants are larger at warmer temperatures. This is an artefact because the hot helium–H_2SO_4 mixture thermally decomposed some of these ions at the highest temperatures at which they could be detected, even though this mixture was never more than 1% of the total helium flow. This is an extreme consequence of the fact that the entire flow tube must be maintained at cold temperatures in order to study certain cluster ions.

The relative rate constants for each temperature are combined to yield relative rate constants for each ion with respect to CO_3^-. For all reactions which did not suffer from obvious thermal decomposition, no temperature dependence was found. Averages were taken when an ion was studied at more than one temperature, with the anomalously high rate constants for $NO_3^-(HNO_3)_2$ and $NO_3^-(HNO_3)_3$ omitted from the averages for these ions. Also included in table 2 is a column labelled k_c, representing the collision rate constants normalized to that for bare CO_3^-. Another column shows the ratio of the relative rate constants to the relative collisional rate constants; these values vary from 0.87 to 1.15. The largest values are for ions that may also suffer a small amount of thermal decomposition. The fact that this range is so narrow indicates that the rate constants are all collisional within a small range. In the last column, we report 300 K rate constants based on the relative rate constants and the collisional value for CO_3^-. The rapidity of the reactions is presumably due to the large gas-phase acidity of H_2SO_4 [66]. The product ions all could be seen to contain HSO_4^- cores with various degrees of solvation. Unfortunately, the degree of solvation could not be determined.

The results are consistent with the previous findings of Viggiano *et al.* except for the reaction of H_2SO_4 with $NO_3^-(HNO_3)_2$. The previous study found a value of only 60% of the collision rate. The new results show no such trend and indicate that $n = 3$ is also fast, arguing against a downturn in the rate constant. However, the previous measurements were taken at 343 K, and the warmest temperature at which $NO_3^-(HNO_3)_2$ was reliably studied in the present set of experiments was 200 K. Normally ion–molecule reactions become faster at lower temperatures; so this may

Table 2. Relative rate constants of chemical ionization primary ions with H_2SO_4, where parentheses indicate the ion whose rate constant the other rate constants are relative to and curly brackets indicate that the rate constant is not used in the average; see text for explanation.

Ion	Relative rate constant at the following temperatures					Relative rate constant			
	300 K	273 K	233 K	200 K	158 K	$\langle k \rangle$[a]	k_c[b]	k/k_c[c]	k_{300}[d] (10^9 cm^3 s^{-1})
CO_3^-	(1)		(1)			(1)	(1)	(1)	(2.39)
$CO_3^-(H_2O)$			0.89	0.90		0.90	0.92	0.98	2.15
$CO_3^-(H_2O)_2$				1.0		1.0	0.87	1.15	2.39
HCO_3^-	1.1					1.1	0.99	1.11	2.63
$HCO_3^-(H_2O)$	0.83		0.82			0.83	0.92	0.9	1.98
$HCO_3^-(H_2O)_2$				0.99		0.99	0.86	1.15	2.37
NO_3^-	0.99	(0.99)	0.95			0.97	0.99	0.98	2.32
$NO_3^-(H_2O)$		0.86	0.85	(0.86)		0.86	0.92	0.94	2.06
$NO_3^-(H_2O)_2$				0.79		0.79	0.87	0.91	1.89
$NO_3^-(H_2O)_3$					0.79	0.79	0.82	0.96	1.89
$NO_3^-(HNO_3)$		0.75		0.80	(0.78)	0.78	0.76	1.03	1.86
$NO_3^-(HNO_3)_2$		{0.87}		0.74	0.69	0.72	0.72	1.00	1.72
$NO_3^-(HNO_3)_3$				{1.1}	0.75	0.75	0.85	0.87	1.79
$NO_3^-(HNO_2)$				0.78		0.78	0.84	0.93	1.86

[a] Average relative rate constants.
[b] Calculated collision rates ratioed to the calculated collision rate for CO_3^-.
[c] Ratio of previous two columns.
[d] Calculated rate constants at 300 K based on the relative rates and assumption that the CO_3^- rate is collisional.

explain the discrepancy [67]. Alternatively, the previous data were taken in a flowing-afterglow instrument in which large amounts of HNO_3 were added. In similar comparisons of selected ion flow tube data with flowing-afterglow data involving clusters, the flowing-afterglow data were shown to be in error because equilibrium processes occur [40, 68]. Tanner and Eisele [69] have concluded that the reactions of $NO_3^-(HNO_3)(H_2O)_n$ ions also did not depend on the level of hydration, consistent with the results taken using the supersonic source on a SIFT.

Both sets of measurements are important for chemical ionization detection of the respective trace neutral. The H_2SO_4 results show that all ions previously used for CIMS detection of H_2SO_4 concentrations in the atmosphere react rapidly with H_2SO_4, producing HSO_4^- core ions. Therefore the assumption of calculating the collision rate constant for the ion of interest with H_2SO_4 has led to little error in previous measurements of H_2SO_4 concentrations. This is in contrast with the SO_2 measurements which show that hydration does affect reactivity. Fortunately most of the $CO_3^-(H_2O)_n$ ions for CIMS measurements of SO_2 involve $1 \leqslant n \leqslant 3$. In this range, the rate constants are insensitive to n and to temperature, which makes deriving SO_2 neutral concentrations easier. We have estimated that using a value of 1.5×10^{-9} cm^3 s^{-1} for the effective rate constant leads to a less than 10% error on any measurement taken at altitudes over 5000 ft. Nevertheless, in our CIMS measurements we now routinely calibrate for SO_2, in part because of the results presented here.

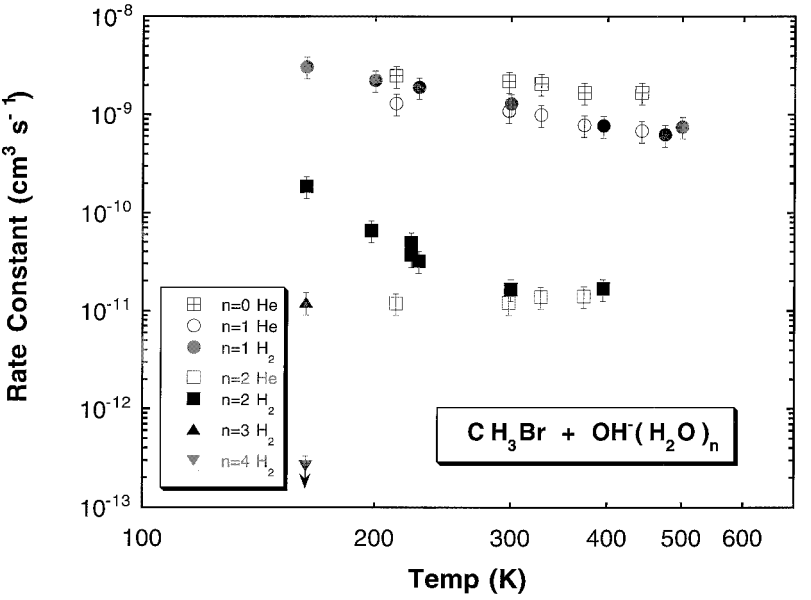

Figure 7. Rate constants for the reactions of $OH^-(H_2O)_n$ with CH_3Br as a function of temperature [68]: (⊞), (○), (□), data taken in a helium buffer; (●), (■), (▲), (▼), data taken in H_2; (⊞), $n = 0$; (○), (●), $n = 1$; (□), (■), $n = 2$; (▲), $n = 3$; (▼), $n = 4$. 25% error limits on each point are shown.

3.3. *Effect of solvation on nucleophilic substitution*

A considerable amount of theoretical and experimental effort has focused on gas-phase bimolecular nucleophilic displacement reactions (S_N2). Our recent work has concentrated on the effects of hydration level and temperature on the rate constants and products of the S_N2 reactions between methyl bromide and the ions $X^-(H_2O)_n$, where X = OH, F or Cl. Our results corroborate certain facets of other experimental [70–75] and theoretical studies [76–80] and call into question others. The main finding, that nucleophilic displacement reactions have rates which decrease with increasing hydration and preferentially lead to unhydrated products, remains unchanged. However, we have found that, in the absence of a fast S_N2 reaction channel, other mechanisms such as association and ligand switching can become important [40, 68]. We have also found some of the details of previous experiments to be in error, demonstrating the advantages of the present technique. We devote the most space to the $OH^-(H_2O)$ series since this is described first and many of the principles are the same for the other series.

3.3.1. *$OH^-(H_2O)_n + CH_3Br$*

The first set of S_N2 reactions that we studied with the supersonic source in the SIFT were the reactions of CH_3Br with $OH^-(H_2O)_n$, $0 \leqslant n \leqslant 4$ [68]. The data are shown as functions of temperature in figure 7. The 300 K and 163 K rate constants are listed in table 3 together with 300 K results from other studies. For $n = 1$ and $n = 2$, the data were taken using both a H_2 buffer (shown as full symbols) and a helium buffer (open symbols). The most pronounced trend is that the reactivity decreases dramatically with increasing cluster size. The reaction of methyl bromide with the unsolvated OH^- ion is fast, approaching the collision rate. However, the rate constants drop by a factor of 10^4 in going from $n = 0$ to $n = 4$. The large dependence on solvation was first

Table 3. Comparison of rate constants for the reaction of $OH^-(H_2O)_n$ with CH_3Br.

	Rate constants ($cm^3\ s^{-1}$)			
n	163 K	300 K	Collision rate constant (300 K)	Previous result (300 K)
0		2.2×10^{-9}	2.79×10^{-9}	1.0×10^{-9} [70] 9.9×10^{-10} [81] 1.9×10^{-9} [82] 2.2×10^{-9} [5]
1	3.1×10^{-9}	1.2×10^{-9}	2.09×10^{-9}	6.3×10^{-10} [70] 1.7×10^{-9} [83]
2	1.9×10^{-10}	1.7×10^{-10}	1.81×10^{-9}	2×10^{-12} [70]
3	1.2×10^{-11}		1.66×10^{-9}	$< 2\times10^{-13}$ [70]
4	$< 2.7\times10^{-13}$		1.56×10^{-9}	

demonstrated by Bohme and co-workers [70, 72] and later by Hierl *et al.* [84]. The rate constants for OH^- show a slight negative temperature dependence, $T^{-0.58}$. The rate constants for $OH^-(H_2O)$ reacting with CH_3Br are slightly smaller than those for unsolvated OH^-, and the temperature dependence for this reaction is $T^{-1.6}$. The addition of one H_2O molecule to the OH^- ion changes the kinetics only slightly. The addition of a second H_2O reduces the rate constants by a factor of about 100 from the rate constant for one H_2O. The $n = 2$ reaction could not be studied above 400 K since this reactant ion thermally decomposes in the flow tube above this temperature. Similarly, we were able to examine the $n = 3$ and the $n = 4$ reactions at only the lowest temperature of the study, 163 K. The reaction of $n = 3$ with CH_3Br is just over ten times slower than the $n = 2$ reaction while the reaction of $OH^-(H_2O)_4$ is a factor of at least 40 slower than the reaction with $OH^-(H_2O)_3$. Thus, solvation greatly decreases the reactivity.

For the unsolvated OH^-, the only product ion observed was Br^-, although proton transfer has been observed at higher energies in a beam study [84]. For the $n = 1$ reaction, two S_N2 product ions were observed:

$$\begin{aligned} OH^-(H_2O) + CH_3Br &\rightarrow Br^- + CH_3OH + H_2O, \quad \Delta H^0 = -30.0 \text{ kcal mol}^{-1}, \\ &\rightarrow Br^-(H_2O) + CH_3OH, \quad \Delta H^0 = -42.6 \text{ kcal mol}^{-1} \text{ [84]}. \end{aligned} \tag{17}$$

The unsolvated Br^- product accounts for approximately 90% of the reactivity, and the branching percentage does not depend on temperature within our experimental uncertainty. The reaction of $OH^-(H_2O)_2$ with CH_3Br has three pathways:

$$\begin{aligned} OH^-(H_2O)_2 + CH_3Br &\rightarrow Br^- + CH_3OH + 2H_2O, \quad \Delta H^0 = -13.6 \text{ kcal mol}^{-1}, \\ &\rightarrow Br^-(H_2O) + CH_3OH + H_2O, \quad \Delta H^0 = -26.2 \text{ kcal mol}^{-1} \text{ [84]}, \\ &\rightarrow OH^-(H_2O)_2(CH_3Br), \quad \Delta H^0 = ?. \end{aligned} \tag{18}$$

The latter channel is not observed in the helium buffer. The branching percentages for the three channels are shown in figure 8 for the data taken in a H_2 buffer. At low temperatures, one clearly sees the onset of an association channel which had not been observed previously [72]. The Br^- channel increases monotonically with increasing temperature, while the $Br^-(H_2O)$ channel has a maximum between 200 and 300 K. Substantially more $Br^-(H_2O)$ is found for the $n = 2$ reaction than for the $n = 1$ reaction. The predisposition toward forming unsolvated species had been observed

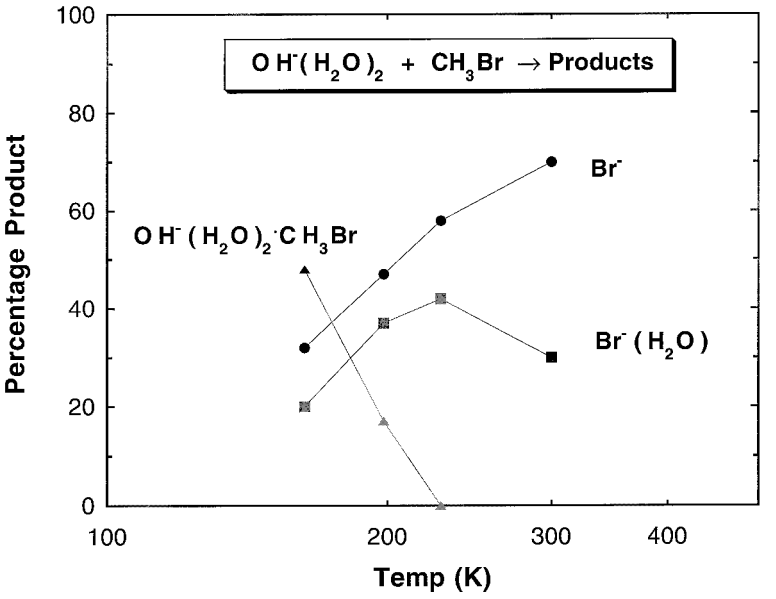

Figure 8. Branching fractions for the reaction of $OH^-(H_2O)_2$ with CH_3Br as a function of temperature expressed as percentages [68]. Only data taken in a H_2 buffer are shown.

previously. Hierl *et al.* [85] explained this by invoking a mechanism that involves a concerted transfer of the solvent during the Walden inversion which is quite unfavourable both energetically and entropically. Regarding the larger reactant ions, the $n = 3$ reaction proceeds exclusively by association, and no product ions were observed for the very slow $n = 4$ reaction.

Although the data taken in helium and H_2 buffers are very similar for the $n = 1$ reaction, the data for the $n = 2$ reaction show significant differences at temperatures below 300 K. The $n = 2$ data taken in a helium buffer show little temperature dependence, with perhaps a slight increase (about 15%) as the temperature increases, while the $n = 2$ rate constants taken in a H_2 buffer show a T^{-4} dependence. The difference between the H_2 and helium buffer data is explained by the presence of the association channel which is observed with the H_2 buffer but not with the helium buffer. Figure 9 illustrates the percentage of the Br^- signal divided by the sum of the Br^- plus $Br^-(H_2O)$ signals for both the helium and the H_2-buffered experiments. For the helium buffer case, this is simply the Br^- branching fraction; for the H_2 buffer, this is the Br^- branching fraction ignoring the association channel. The room-temperature data points agree extremely well and, at low temperatures, the H_2 buffer data show a slightly higher fraction of Br^- than observed in the helium case. It appears that the Br^- channel levels out at lower temperatures.

For the reaction of $OH^-(H_2O)$ with CH_3Br, eight isotopic variants were studied: $OH^-(H_2O)$ with zero to three deuterium atoms reacting with both CH_3Br and CD_3Br. The results are listed in table 4. The results are relative rate constants with the rate constant for the fastest reaction set equal to one. The relative rate constants for deuterium substitution in the ion are very accurate since the rate constants were taken simultaneously. For each temperature and for both CH_3Br and CD_3Br, the reaction with $H_2DO_2^-$ which could be $OH^-(HOD)$ or $OD^-(H_2O)$ was found to have the largest rate constant. We found little variability with condition and therefore also report the

Table 4. Isotopic study of the $OH^-(H_2O)+ CH_3Br$ reaction. The rate constants for a given isotopic variant of $OH^-(H_2O)$ are reported relative to the rate constant for $H_2DO_2^-$ listed in the last column.

Temperature (K)	Neutral	Relative rate constant				$k(H_2DO_2^-)$ ($cm^3\ s^{-1}$)
		$H_3O_2^-$	$H_2DO_2^-$	$HD_2O_2^-$	$D_3O_2^-$	
200	CH_3Br	0.92	1.00	0.98	0.91	2.45 (− 9)
	CD_3Br	0.94	1.00	0.99	0.95	2.38 (− 9)
300	CH_3Br	0.90	1.00	0.97	0.89	1.44 (− 9)
	CD_3Br	0.88	1.00	0.96	0.84	1.54 (− 9)
500	CH_3Br	0.91	1.00	0.98	0.91	8.30 (− 10)
	CD_3Br	0.93	1.00	1.00	0.92	7.99 (− 10)
Average all conditions		0.91	1.00	0.98	0.90	

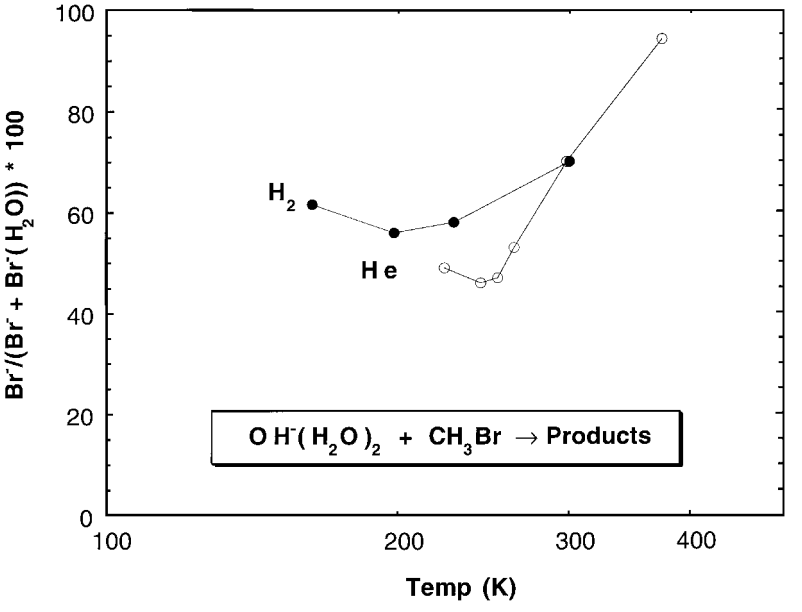

Figure 9. The Br^- fraction divided by the sum of the Br^- plus $Br^-(H_2O)$ fractions for the reaction of $OH^-(H_2O)_2$ with CH_3Br as a function of temperature [68]: (●), data taken in H_2 buffer; (○), data taken in helium buffer.

average isotope effect for all conditions. We found no difference between CH_3Br and CD_3Br, the average ratio of rate constants for these neutrals being 1.00± 0.03. It was not possible to determine accurately the product distribution for the various isotopes. Deuterium substitution in $H_3O_2^-$ showed a larger variation. In all cases the reactivity order was $H_2DO_2^- \geqslant HD_2O_2^- > H_3O_2^- \geqslant D_3O_2^-$, except for the 200 K data for CD_3Br where the order for the last two was reversed but only by 1%. The ions group into two categories, those incorporating both hydrogen and deuterium and those with only hydrogen or deuterium. The former group reacts about 10% faster than the latter group. This result is quite unique and remains unexplained.

The small negative temperature dependence of the rate constant reported here for the nucleophilic displacement reaction between OH^- and CH_3Br has been seen in previous studies for comparable S_N2 reactions such as the reactions of F^- with the

methyl halides [86] and OH^- with CH_3Cl [85]. Two factors are thought to contribute to this behaviour. First, the rate constant for the collision of an ion with a polar molecule is a gradually decreasing function of temperature. Second, theoretical considerations predict [87–94] that the reaction efficiency (i.e. fraction of collisions resulting in product formation) will be a decreasing function of temperature for exothermic nucleophilic displacement at an sp^3 carbon atom. These predictions, based upon the double-well potential model first proposed by Olmstead and Brauman [82,70], assume that the reaction efficiency at a given temperature is the consequence of the competition between two pathways for the unimolecular decay of the reactant adduct ($OH^- \cdot CH_3Br$, in this case): dissociation back to reactants or transformation to the product adduct ($Br^- \cdot CH_3OH$). Since dissociation back to reactants involves a looser transition state and hence a higher density of states than does the forward transformation, the rate constant for the backward reaction increases more rapidly with increasing temperature than does that for the forward reaction. Consequently, a decreasing fraction of the collision adducts will surmount the central barrier and result in product formation with increasing temperature. This effect has been modelled quantitatively [95].

The two principal consequences of reactant solvation, namely the reduction of the rate constant and its altered temperature dependence, are also consistent with the predictions of the double-well model. These effects are discussed in turn.

Solvation of the ionic reactant without comparable solvation of the ionic product reduces the reaction exothermicity and stabilizes the reactants more than it does the transition state corresponding to the central barrier in the reaction coordinate (i.e. the energy difference ΔE_0 between this transition state and the reactants becomes less negative). At a given temperature, this decrease in the magnitude of $-\Delta E_0$ will increase the fraction of reaction adducts which dissociate backwards to regenerate the reactants at the expense of those which surmount the central barrier and are transformed into product adducts. This suggests a decreasing reaction efficiency with increasing reactant solvation, as is observed in figure 7. We have reported similar behaviour for the reactions of $OH^-(H_2O)_{0-2}$ with CH_3Cl [85]. The CH_3Cl rate constants also decrease with increasing reactant solvation, the decrease being even larger than that found for the reaction of $OH^-(H_2O)_n$ with CH_3Br. We attribute this latter observation to the fact that the reaction of OH^- with CH_3Cl is less exothermic (and hence more sensitive to reactant stabilization) than is the reaction with CH_3Br.

The same model explains the gross features of the temperature dependences of the S_N2 rate constants with increasing reactant solvation. At first, reactant solvation makes E_0 less negative, which causes the temperature dependence of the reaction efficiency (and hence of the overall reaction rate constant) to become more negative. This is what is observed in the $OH^-(H_2O)_n$ reactions with CH_3Br in going from $n = 0$ (where $k \propto T^{-0.58}$) to $n = 1$ (where $k \propto T^{-1.6}$). With further reactant solvation, E_0 passes through zero and then becomes positive, causing the temperature dependence of the reaction efficiency to become flat and then positive. The onset of this behaviour is demonstrated by the levelling out of the $n = 2$ temperature dependence. The strong negative temperature dependence for the $n = 2$ reaction in H_2 buffer below 250 K is typical for association reactions, and it mainly reflects the temperature dependence of the collision complex lifetime [27]; thus, it is irrelevant to the present discussion of the temperature dependence of the S_N2 reaction channel.

The difference between the helium and H_2 buffer data for the $n = 2$ reaction is connected to the onset of the association channel. On close examination the large rate

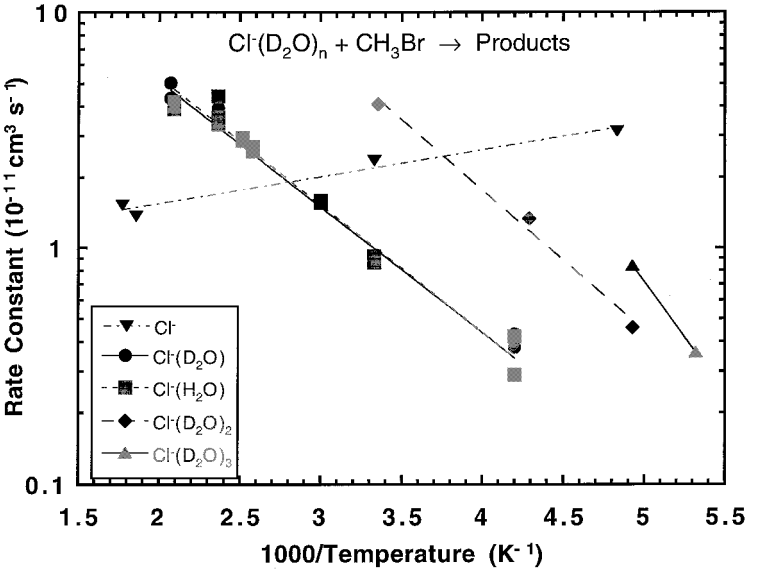

Figure 10. Arrhenius plot of the rate constants for the reactions of CH_3Br with $Cl^-(H_2O)$ and $Cl^-(D_2O)_n$, $0 \leqslant n \leqslant 3$ [40].

constants observed in the hydrogen buffer are found at temperatures where the association channel is negligible. This shows that the bimolecular rate constants at low temperatures in the hydrogen buffer are affected by collisions with the buffer gas. In other words, the complex lives long enough to undergo collisions with the buffer gas, which in turn increases the rate constant. The onset of the association channel at just slightly lower temperatures guarantees that the complex lifetime is at least of the order of the collision time scale with the buffer gas, about 10^{-7} s.

The influence of the buffer gas on an S_N2 reaction has been observed by Giles and Grimsrud [96] in the reaction of Cl^- with CH_3Br. In that reaction, increasing pressure increases the rate constant, and this is consistent with our data. H_2 is more efficient at transferring energy than is helium. Therefore the effects of increasing pressure would be seen in a H_2 buffer [97–99] before they would be observed in helium, and the effect would be to increase the rate constant. The increase in the H_2 data relative to the helium data does not necessarily mean that no collisions of the complex with helium take place but rather that the helium collisions are less efficient in transferring energy from the complex. Helium is known to be a very inefficient third body [97–99].

3.3.2. $Cl^-(D_2O)_{0-3} + CH_3Br$

Rate constants measured using the SIFT for the reactions of $Cl^-(H_2O)$ and $Cl^-(D_2O)_n$, $0 \leqslant n \leqslant 3$, with CH_3Br are shown in figure 10 [40]. Rate constants for the reaction of the unsolvated Cl^- are taken from a previous study [100] although we remeasured these rate constants at several temperatures and obtained excellent agreement with these previous results. The gas-phase S_N2 reaction of $Cl^- + CH_3Br$ has been well studied experimentally and theoretically [81–83, 92, 100–107]; the reaction produces only Br^- and shows the typical S_N2 negative temperature dependence [67, 91, 92].

Studies [73, 108] on the effects of solvation on the reaction of Cl^- with CH_3Br have

Table 5. Experimental product percentages for the reaction of $Cl^-(D_2O) + CH_3Br$.

Temperature (K)	Experimental value[a] (%)		
	Br^-	$(BrCH_3Cl)^-$	$(BrCH_3Cl)(D_2O)$
241	77	20	3
273	88	12	—
298	94	6	—
328	98	2	—
363	99	1	—

[a] Does not include the Cl^- channel.

found that the addition of a variety of organic solvent molecules to Cl^- greatly reduces the reaction rate. In our study, we found that adding a single water molecule to Cl^- changes the temperature dependence from negative to positive, the first time that this has been observed in this type of reaction. In addition, no H_2O–D_2O isotope effect was observed. The $n = 1$ reaction is well described by the Arrhenius equation with an activation energy of 10.3 kJ mol^{-1}. The reactions of $Cl^-(D_2O)_{2,3}$ also exhibit positive temperature dependences well described by an Arrhenius equation; the activation energy for the $n = 2$ reaction is 11.5 kJ mol^{-1}.

Unlike the $OH^-(H_2O)_n$ system discussed previously, where hydration of the reactant ion effectively slows down the overall reaction with methyl bromide, we found that hydration has only a small effect on overall reactivity and that the reaction mechanism changes from nucleophilic displacement (S_N2) to ligand switching. Three product ions were observed for the $n = 1$ reaction:

$$\begin{aligned} Cl^-(H_2O) + CH_3Br &\rightarrow Br^- + CH_3Cl + H_2O, \quad \Delta H = +\ 25 \text{ kJ mol}^{-1}, \\ &\rightarrow Cl^-(CH_3Br) + H_2O, \quad \Delta H = +\ 9.6 \text{ kJ mol}^{-1} \\ &\rightarrow Cl^-(H_2O)(CH_3Br), \quad \Delta H = ?. \end{aligned} \tag{19}$$

We write the product as $Cl^-(CH_3Br)$ and not $Br^-(CH_3Cl)$ for reasons given below. Table 5 gives the observed product fractions as a function of temperature. It is possible that Cl^- is an additional minor product of reaction (19), although the branching percentage could not be quantified. Although the main product ion is Br^-, we were able to show that the reaction mechanism is

$$Cl^-(D_2O) + CH_3Br \rightarrow Cl^-(CH_3Br) + D_2O, \tag{20}$$

followed by thermal dissociation of $Cl^-(CH_3Br)$:

$$\begin{aligned} Cl^-(CH_3Br) + He &\rightarrow Br^- + CH_3Cl + He, \\ &\rightarrow Cl^- + CH_3Br + He. \end{aligned} \tag{21}$$

Several facts led to question that the Br^- channel was due to nucleophilic displacement. The lack of an isotope effect suggests that an S_N2 mechanism is not operative; O'Hair *et al.* [75] found significant isotope effects in the S_N2 reactions of $F^-(H_2O)$ and $F^-(D_2O)$ with methyl halides. More importantly, the 10.3 kJ mol^{-1} activation energy observed for the $n = 1$ reaction most closely matches the endothermicity of the ligand switching reaction to form $Cl^-(CH_3Br)$ which is substantially lower than the endothermicity of the S_N2 channel producing Br^-. Nucleophilic displacement to form $Br^-(H_2O)$ is allowed, but none was observed.

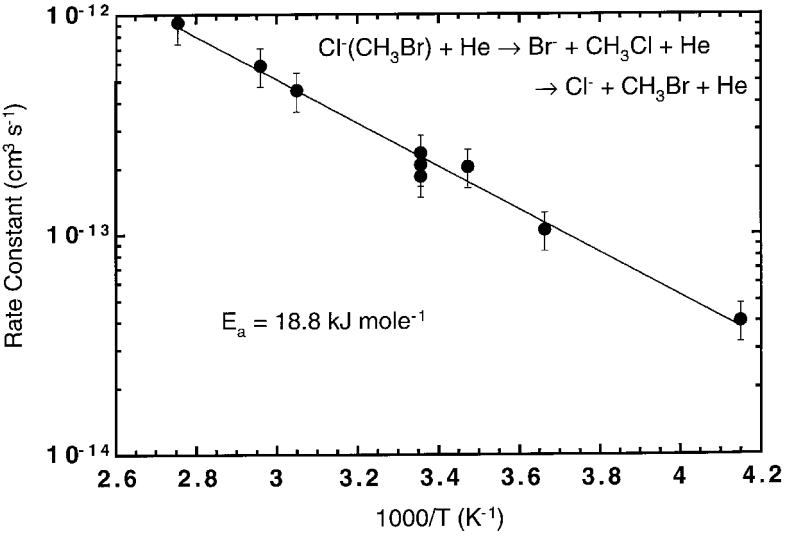

Figure 11. Arrhenius plot of the first order rate constant for the decomposition of $Cl^-(CH_3Br)$ [40].

To test the proposed two-step mechanism, D_2O was added to the helium buffer in sufficient quantities to allow the exothermic ligand exchange reaction

$$Cl^-(CH_3Br) + D_2O \rightarrow Cl^-(D_2O) + CH_3Br \qquad (22)$$

to scavenge some of the $Cl^-(CH_3Br)$ before it could undergo thermal dissociation (reaction (21)) but not enough to affect the initial Cl^- to $Cl^-(D_2O)$ ratio. With added D_2O, the slope of the decay of the $Cl^-(D_2O)$ signal is a factor of 3.5 less than without added D_2O, indicating that $Cl^-(D_2O)$ is regenerated by reaction (22). In addition, the Br^- and $Cl^-(CH_3Br)$ signals are both reduced when D_2O is added. Similar results were obtained for a variety of D_2O concentrations. These results all support the proposed mechanism showing that the direct S_N2 channel is small or non-existent. The fact that D_2O scavenges the dissociating complex to form $Cl^-(D_2O)$ also shows that the complex is correctly written as $Cl^-(CH_3Br)$ and not as $Br^-(CH_3Cl)$.

The break-up rate of the $Cl^-(CH_3Br)$ complex (reaction (21)) was determined from the $Cl^-(D_2O)$ and $Cl^-(CH_3Br)$ signals obtained as a function of $[CH_3Br]$ (in the absence of added D_2O). We used a variable-step fourth-order Runge–Kutta algorithm to integrate the rate equations resulting from reactions (20) and (21) as a function of $[CH_3Br]$. The resulting thermal dissociation rate constants for reaction (21) are shown in figure 11 as an Arrhenius plot. We estimated that the rate constants have an absolute accuracy of ± 40% and a relative accuracy of ± 20%. The dissociation rate constant is well described by the Arrhenius equation with an activation energy of 18.8 kJ mol^{-1}. The error in the activation energy is estimated as ± 2.5 kJ mol^{-1} based on taking the 20% error at the lowest and highest temperatures.

We also used this approach to estimate the dissociation branching fractions of the Br^- and Cl^- product channels of reaction (21). In this case we included the effect of the reaction of Cl^- with methyl bromide:

$$Cl^- + CH_3Br \rightarrow CH_3Cl + Br^-. \qquad (23)$$

This analysis indicated the fraction of Br^- produced from reaction (21) was 90%, and

the fraction of Cl^- produced was 10%. However, it is probable that a small portion of $Cl^-(D_2O)$ and $Cl^-(CH_3Br)$ clusters break up upon sampling to produce Cl^-. If sampling break-up is also included in the model, then equally good fits are obtained for 100% of the reaction proceeding via the Br^- channel with a 4% break-up upon sampling. Thus, our data place limits on the Cl^- formation channel at 0–10%.

For both larger reactant ions, $n = 2$ and $n = 3$, the main ionic product was $Cl^-(D_2O)_{n-1}$, and no hydrates of Br^- were observed. By analogy to the $n = 1$ reaction, we propose the following two-step mechanism for the reactions of $Cl^-(D_2O)_{2,3}$:

$$Cl^-(D_2O)_n + CH_3Br \rightarrow Cl^-(D_2O)_{n-1}(CH_3Br) + D_2O, \quad (24)$$

$$Cl^-(CH_3Br)(D_2O)_{n-1} + He \rightarrow Cl^-(D_2O)_{n-1} + CH_3Br + He,$$

$$\rightarrow Cl^-(D_2O)_{n-2}(CH_3Br) + D_2O + He. \quad (25)$$

The temperature dependence of these products is consistent with the proposed mechanism, that is reaction (23) is considerably slower at lower temperatures.

Thus, for the $Cl^-(D_2O)_n + CH_3Br$ system, we find that the S_N2 mechanism is only important for $n = 0$. For $n > 0$ we observe ligand switching presumably because the relative height of the central barrier becomes too high for the S_N2 mechanism to be efficient. This result is to be expected because the barrier crossing efficiency for the $n = 0$ case is already quite low (1%), and the relative height of the central barrier is believed to increase with increasing hydration level [70]. Indeed, this is what is observed in the $OH^-(H_2O)_n$ and $F^-(H_2O)_n$ systems.

Ligand switching mechanisms had not been previously reported for the reactions of hydrated ions with methyl halides. However, previous studies have mostly focused on reactions involving F^- or OH^-. At low levels of hydration, F^- and OH^- form substantially stronger bonds with water than does Cl^- [109]. As a result, ligand switching with hydrates of F^- and OH^- is probably much more endothermic. The *ab initio* studies of Morokuma [76] and Ohta and Morokuma [77] support this statement. They calculated that the reaction $OH^-(H_2O) + CH_3Cl \rightarrow Cl^-(CH_3Cl) + H_2O$ is endothermic by 57 kJ mol^{-1}, while the reaction $Cl^-(H_2O) + CH_3Cl \rightarrow Cl^-(CH_3Cl) + H_2O$ is endothermic by only 4 kJ mol^{-1}. It is interesting to note that, as the hydration level of F^-, OH^- and Cl^- are increased, their water binding energies become similar. Thus, it is possible that ligand switching reactions will be observed for large ($n > 3$) hydrates of F^- and OH^-. Indeed we have found this to be the case for F^- as discussed below.

Two other studies of solvated chloride ions with methyl bromide have been made. Bohme and Raksit [73] studied the reactions of $Cl^-(S)_n$ with CH_3Br, where S = CH_3OH, C_2H_5OH, CH_3COCH_3, HCOOH and CH_3COOH. They found that the reaction rate constants were too low for accurate measurement for $n \geqslant 1$ and did not observe ligand switching. Giles and Grimsrud [108] found that solvation of Cl^- by $CHCl_3$ also inhibits the reaction with CH_3Br and similarly did not find evidence for ligand switching. However, the experimental systems used in these studies produced solvated clusters by adding solvent directly to the reaction mixture. Hence, any $Cl^-(S)_{n-1}CH_3Br$ produced would be quickly converted back into $Cl^-(S)_n$ by the high levels of solvent in the flow since the ligand switching is exothermic in that direction (analogous to reaction (25)).

Probably the most interesting aspect of this study was unexpected, namely the ability to study the thermal dissociation of $Cl^-(CH_3Br)$. We found that when the complex is formed via $Cl^-(H_2O) + CH_3Br$, it dissociates through the Br^- channel with a branching fraction greater than 90%. This is because the endothermic process drops

this into low-energy states of the complex, and the least exothermic dissociation pathway is the formation of Br^-. Several previous studies have also focused on the $Cl^-(CH_3Br)$ complex because of its role as the initial intermediate in the unsolvated $Cl^- + CH_3Br$ reaction. At a low pressure (0.4 torr) the $Cl^- + CH_3Br$ reaction proceeds at 1% of the collision rate. Thus, 99% of the $Cl^-(CH_3Br)$ collision complexes dissociate back into Cl^- and CH_3Br, while only 1% of the complexes dissociate into Br^- and CH_3Cl. At a high pressure (N_2 at 640 torr) the reaction proceeds at 3% of the collision rate, which corresponds to the dissociation of 97% of the complexes to Cl^- and CH_3Br. Increasing pressure means that collisions occur during the lifetime of the complex and cool the ion leading to more Br^-. Collision-induced dissociation experiments [104] lead to roughly 50% Br^-, and metastable decay experiments [103, 110] of long-lived (approximately microsecond) complexes almost exclusively form Br^-.

Because the $Cl^-(CH_3Br)$ is formed by ligand switching, it is formed quite cold, and its dissociation in the bath gas could then be modelled by Rice–Ramsperger–Kassel–Marcus (RRKM) theory [40]. Since the barrier height is very critical to this calculation and not accurately known, it was left as an adjustable parameter and determined by the fit that best matched the temperature dependence. The barrier height that best matched the data was 22.5± 2.5 kJ mol^{-1}. The RRKM calculations showed that little Cl^- forms, consistent with our estimates. The barrier height derived this way is considerably less (about 15 kJ mol^{-1}) than the barrier found in *ab initio* calculations [107] or derived from the bimolecular reaction from statistical modelling [103, 110, 111]. Several factors may contribute to this discrepancy.

(1) *Ab initio* calculations involving atoms as heavy as bromine are often in error especially for a transition state.
(2) The barrier derived from the bimolecular rate constant assumes statistical behaviour, and both experiments and theory indicate that this reaction is not statistical.
(3) Tunnelling may be occurring in the thermal dissociation reaction owing to the long time scale involved.

The results do show that RRKM modelling can accurately predict the temperature dependence using the 22.5 kJ mol^{-1} barrier. This is in contrast with the statistical calculation of the bimolecular rate constant between Cl^- and CH_3Br for which the temperature dependence of the rate constant cannot be accurately predicted [111].

Assuming that the barrier is as calculated from the thermal dissociation experiments, the following picture of the reaction emerges. For the bimolecular reaction, the lifetime of the complex is short (approximately picoseconds), non-statistical behaviour occurs, and most of the dissociation of the complex is back into reactants, namely Cl^-. As the energy of the complex decreases, the lifetime increases until a lifetime of microseconds is found in metastable decay experiments. The RRKM calculations show that, when the lifetime is long, the reaction behaves statistically, possibly with an effective barrier set by tunnelling. The postulate that statistical theories describe nucleophilic displacement reactions when the lifetime is long and do not when the lifetime is short is both reasonable and what we have observed previously in reactions were internal energy dependences have been examined [112].

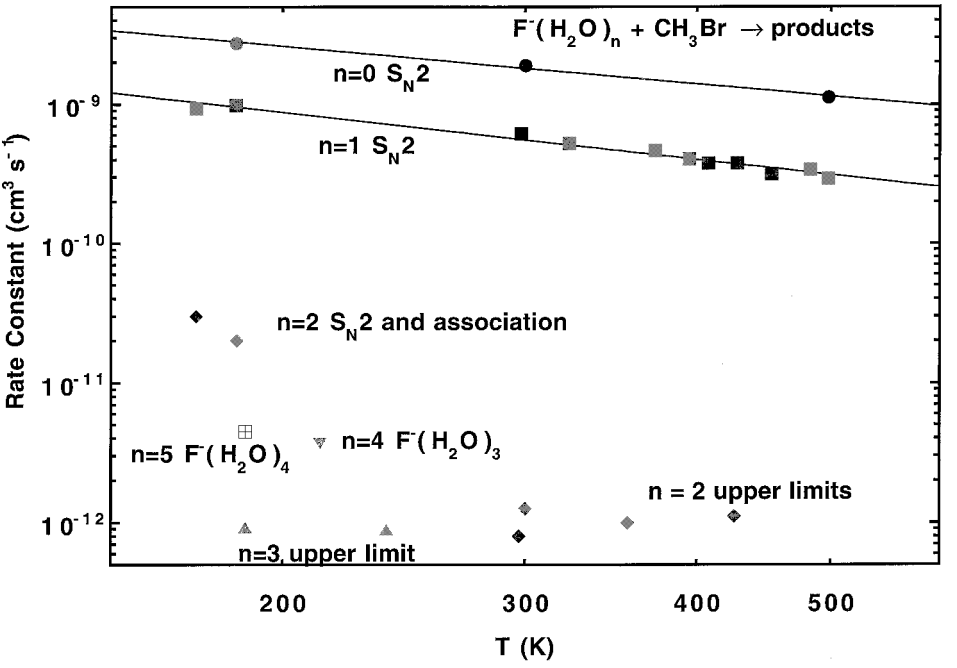

Figure 12. Rate constants for the reactions of $F^-(H_2O)_n$ plus CH_3Br as a function of temperature [113]: (●), $n = 0$; (■), $n = 1$; (◆), $n = 2$; (▲), $n = 3$; (▼), $n = 4$; (⊞), $n = 5$.

3.3.3. $F^-(H_2O)_{0-5} + CH_3Br$

We have also studied the reactions of CH_3Br with $F^-(H_2O)_n, 0 \leqslant n \leqslant 5$ [113]. All features found in this series of reactions are similar to those found in either of the two proceeding series and this discussion will therefore be relatively short. Figure 12 shows rate constants measured in the SIFT for the reaction of CH_3Br with $F^-(H_2O)_n, 0 \leqslant n \leqslant 5$, as functions of temperature. The addition of one water molecule to the bare fluoride ion decreases the reaction rate by a factor of three. The addition of the second water solvent decreases the rate by a factor of greater than 40, and the third water molecule makes the rate immeasurably slow. This decrease in S_N2 reactivity is similar to that observed for CH_3Br reaction with $OH^-(H_2O)_n$ ions. For the bare fluoride ion, a $T^{-0.9 \pm 0.1}$ dependence was found when a power-law expression was fitted to the data, while the temperature dependence for the $n = 1$ ion is slightly more negative, $T^{-1.1 \pm 0.05}$. Rate constants were measured for both $F^-(H_2O)$ and $F^-(D_2O)$. Although the $F^-(D_2O)$ reaction is about 25% faster than the $F^-(H_2O)$ reaction, a similar temperature dependence was observed. The reaction of CH_3Br with $n = 2$ was so slow at temperatures greater than room temperature that only an upper limit could be determined for the rate constant, a value consistent with the upper limit reported by Bohme and Raksit [73]. At lower temperatures the $n = 2$ rate constants are large enough for measurement but remain a factor of 40 smaller than the $n = 1$ rate. For $n = 3$, the reaction is so slow that only an upper limit could be placed on the rate. Interestingly, the reactions of CH_3Br with even larger reactant ions, $n = 4$ and $n = 5$, are faster than the $n = 3$ reaction.

A previous study by Bohme and Raksit [73] reported the $n = 1$ rate to be a factor of almost ten smaller than the $n = 0$ rate, a much greater reduction than found here.

However, the measurements by Bohme and Raksit [73] were performed in a flowing-afterglow apparatus that had several F^- hydrates present simultaneously. Presumably, the $n = 1$ and $n = 2$ clusters were in equilibrium, and the $n = 1$ rate was influenced by the presence of the extremely slow $n = 2$ reaction. More recently, O'Hair *et al.* [75] found values about 20% lower than our results but well within the combined error limits.

For the reactions of CH_3Br with $F^-(H_2O)_n$, $0 \leqslant n \leqslant 3$, we find Br^- to be the major ion product with a smaller amount of $Br^-(H_2O)$ also being formed (always less than 25% and decreasing with increasing temperature). The only observed ionic product for the $n = 0$ reaction was Br^-, while two ionic products are observed for the $F^-(H_2O)$ reaction, Br^- and $Br^-(H_2O)$:

$$\begin{aligned} F^-(H_2O) + CH_3Br &\rightarrow Br^- + CH_3F + H_2O, \quad \Delta H^0 = -76 \text{ kJ mol}^{-1}, \\ &\rightarrow Br^-(H_2O) + CH_3F, \quad \Delta H^0 = -128 \text{ kJ mol}^{-1}. \end{aligned} \tag{26}$$

The percentage of Br^- increases from about 80% at low temperatures to essentially 100% at 500 K, and slightly more Br^- is found for $F^-(D_2O)$ than for $F^-(H_2O)$. While the percentage of Br^- formed is similar to that found in the reaction of $OH^-(H_2O)$ with CH_3Br, the temperature dependence of the branching into Br^- is not similar. The former was temperature independent. The F^- results are more intuitive in that less of the cluster product is observed at higher temperatures. As the temperature is raised, the dissociating complex has more energy and therefore one would expect less of the cluster to be formed. No explanation for the difference has been found to date.

For the $n = 2$ reaction, three product channels were observed:

$$\begin{aligned} F^-(H_2O)_2 + CH_3Br &\rightarrow Br^- + CH_3F + 2H_2O, \quad \Delta H^0 = -6 \text{ kJ mol}^{-1} \\ &\rightarrow Br^-(H_2O) + CH_3F + H_2O, \quad \Delta H^0 = -59 \text{ kJ mol}^{-1}, \\ &\rightarrow F^-(H_2O)_2CH_3Br, \quad \Delta H^0 = ?. \end{aligned} \tag{27}$$

The branching percentages at low temperatures were 68% Br^-, 4% $Br^-(H_2O)$ and 28% $F^-(H_2O)_2(CH_3Br)$. The reaction of $n = 3$ is so slow that product branching fractions could not be determined. For both $n = 4$ and $n = 5$, the only observed ionic products were $F^-(H_2O)_{n-1}$. This is due to a mechanism similar to that shown in reactions (24) and (25). The rate-determining step is likely to be the ligand-switching step which would be slightly endothermic, thereby resulting in the small rate constant. The thermal decomposition step is fast enough to keep the concentration of $F^-(H_2O)_{n-1}(CH_3Br)$ at undetectable levels.

Summarizing, hydration changes the mechanism twice in the reaction of CH_3Br with $F^-(H_2O)_n$. Nucleophilic displacement is the only mechanism for $n = 0$ and $n = 1$. The $n = 2$ reaction shows competition between nucleophilic displacement and association. No measurable reaction occurs for $n = 3$, and the $n = 4$ and $n = 5$ reactions occur by ligand switching followed by thermal dissociation. It is somewhat surprising that F^- hydrates ligand switch with CH_3Br while OH^- hydrates do not. One possible explanation is that ligand switching is more endothermic for the OH^- case because the hydration energies of OH^- are greater than those of F^- and/or because the methyl bromide complexation energy of OH^- is less than that of F^-. Small energy differences, of the order of 5 kJ mol^{-1}, would be sufficient to cause ligand switching to be observed for F^- and not for OH^-. The existing experimental [109, 114] and theoretical [115–119] data, while indicating that the relevant energies for F^- and OH^- are similar, are not sufficiently accurate to test this explanation.

All three series of reactions show that, as the nucleophilic displacement channel

becomes inefficient, association or endothermic ligand switching reaction channels can become important. Neither of these channels had been observed previously. The observation of ligand switching followed by thermal dissociation is in essence catalytic decomposition of a ligand and would be hard to observe without the mass selectivity of the present instrumentation.

3.4. *Cluster reactivity as a probe of structure*

The structures of relatively large ion–molecule clusters have been calculated via *ab initio* methods [115, 120–123], molecular dynamics simulations [124–129] and classical electrostatic solvation models [130]. In the case of halide–water clusters $X^-(H_2O)_n$ where X = F, Cl, Br or I, the different theoretical methods all reproduce the stabilization energies that have been measured using high-pressure mass spectrometry [114, 131, 132] and photoelectron spectroscopy [133, 134]; however, the equilibrium geometries generated by the various models are often in conflict. The main difference is whether the halide ion is located on the surface or within the interior of the cluster. Presumably, clusters which contain only a few solvent molecules cannot fully shield the halide core ion and are, by default, surface state clusters. However, with increasing solvation it becomes possible for the halide ion to reside within the cluster's interior, surrounded by a shell of solvent molecules.

We have attempted to utilize size-dependent kinetic data to observe the transition from surface to interior states in halide–water clusters and in $OH^-(H_2O)_n$ clusters. If the assumption is made that surface solvated states react much more rapidly than internally solvated states, then the kinetic data should yield information about the structure of these clusters. This is a reasonable assumption since a strong interaction between a reactant molecule and the ion-molecule cluster is more likely if the reactant molecule can readily access the core ion and become polarized.

We have measured size-dependent rate constants for the reactions of $X^-(H_2O)_n$ (X = F, Cl, Br or I) with Cl_2 at 140 K ; the results are presented in figure 13 [135]. The substantial decrease in the $F^-(H_2O)_n$ rate constants at $n \geqslant 4$ suggests that F^- switches from a surface to internally solvated state at that cluster size. This is in excellent agreement with both the *ab initio* calculations and the molecular dynamics simulations which predict that fluoride clusters will be in surface states for $n \leqslant 3$ and in interior states for $n \geqslant 4$. For the $Cl^-(H_2O)_n$ clusters, the kinetics results indicate that the transition to an internally solvated state occurs at $n = 6$. This agrees well with the *ab initio* calculations but not with the molecular dynamics simulations. *Ab initio* calculations of $Cl^-(H_2O)_n$ clusters predict surface states will be favoured for $n \leqslant 5$ and interior states will be favoured for $n \geqslant 6$, while the molecular dynamics simulations predict surface states will be favoured up to at least $n = 15$. For Br^- and I^- solvated clusters, the kinetics results show no change in the reaction rate constants even for the largest clusters studied ($n = 16$ and $n = 13$ respectively), which suggests that there is no obvious transition from surface to internal solvated states by those cluster sizes. This result is in good agreement with the molecular dynamics simulations and classical electrostatic solvation models, but in disagreement with the *ab initio* calculations. Unlike the *ab initio* calculations, which predict the transition to occur by $n = 6$, the molecular dynamics simulations predict surface states will be favoured up to at least $n = 15$, and the classical electrostatic solvation models for I^- clusters indicate that surface states will be favoured for clusters containing as many as 60 solvent molecules.

Our conclusion that the hydration shells of F^- and Cl^- clusters close before those of Br^- and I^- is quite plausible. For an interior state to be favoured, the halide–water

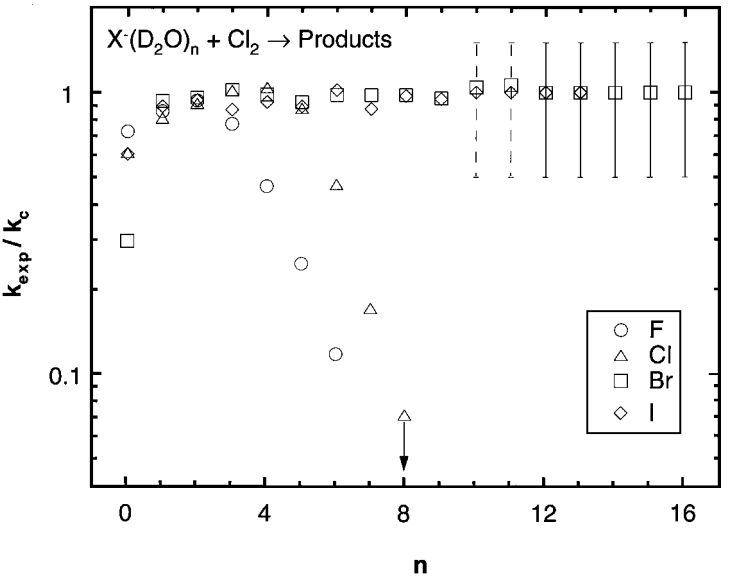

Figure 13. Normalized rate constants for the reactions $X^-(D_2O)_n + Cl_2 \rightarrow$ products at $T =$ 140 K with H_2 as a carrier gas [135]. Experimentally obtained rate constants k_{exp} are divided by the Langevin collision rate constant k_c. Error estimates are 25% accuracy and 15% precision when error bars are not shown. The $Br^-(D_2O)_n$ rate constants for $n \geqslant 12$ and the $I^-(D_2O)_n$ rate constants for $n \geqslant 10$ were not directly determined and have a factor of two uncertainty represented by the error bars (the broken lines for $n = 10$ and $n = 11$ are error bars for I^- only).

interactions must be stronger than the water–water interactions. As the size of the halide ion increases, the electric field that it produces weakens and hence the strength of its electrostatic interaction with water weakens.

With regard to $OH^-(H_2O)_n$ clusters, *ab initio* calculations suggest that interior solvation of the subion develops with four to six water molecules [121]. Size-dependent kinetic data are available for $OH^-(H_2O)_n$ clusters reacting with CO_2 and with HBr. Once again, observing the transition from surface solvated states to internally solvated states is based upon the assumption that surface states react much more rapidly than internal states. Yang and Castleman [35] studied the reactivity of $OH^-(H_2O)_n$ clusters with CO_2 and found that the rate constants for $1 \leqslant n \leqslant 3$ are at the collisional limit, while the rate constants for $n \geqslant 4$ decreased substantially with increasing levels of hydration. The apparent transition in the kinetic data from surface to internally solvated states is in good agreement with the *ab initio* results. Rate constants for the reactions of $OH^-(H_2O)_n$, $0 \leqslant n \leqslant 11$, with HBr at 100 K have been measured in our laboratory, and the results are shown in figure 14 [136]. For $n \leqslant 7$, the reactions with HBr proceed at the gas-phase collision limit. With further solvation, the efficiency of the reaction gradually decreases until it is only one third the collisional rate at $n = 11$. The apparent transition between surface and internal states in this study occurs at somewhat larger cluster sizes than was indicated by the *ab initio* results and the previous kinetic study. We believe that this is because HBr, unlike CO_2, has a relatively large permanent dipole, which allows it to interact more easily with a partially shielded OH^-; that is the polar HBr reactant may burrow through a small number of water molecules to find the ionic core while the non-polar CO_2 could not.

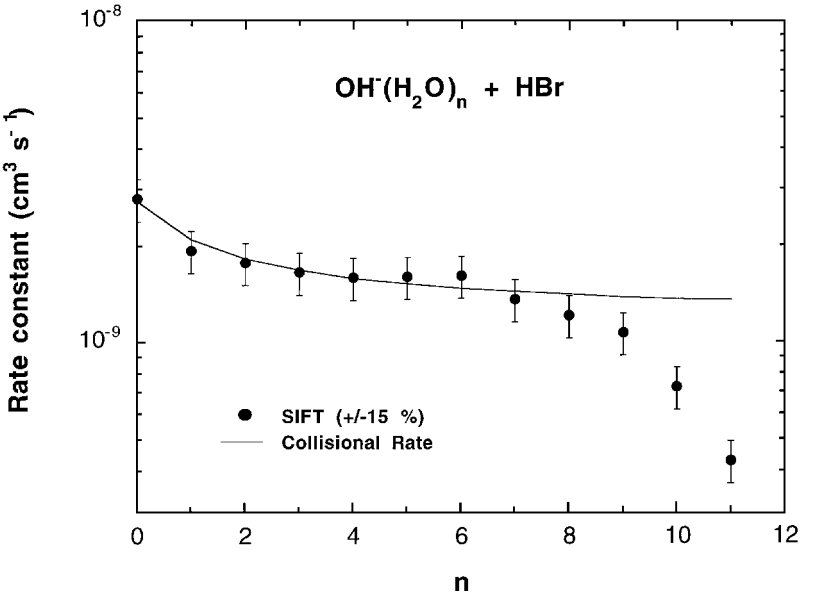

Figure 14. Rate constants for the reactions of $OH^-(H_2O)_n$ with HBr at 100 K, shown as a function of cluster size for $0 \leqslant n \leqslant 11$ [136]: (——), collision rate constants. Error bars reflect relative error only.

4. Conclusions

The addition of a supersonic ion source to a variable-temperature SIFT has proven to be an important addition to the arsenal of experiments employed to study reactions of ionic clusters. The studies done to date have yielded important new data on a variety of processes, some of which could not be studied in any other way at present. While only negative-ion studies have been reported thus far, we are now in the process of making the first measurements with positive cluster ions, and it appears that we shall be able to study an interesting variety of positive ions.

Thermal dissociation processes have proven to be important in a variety of ways. Thermal dissociation sets the upper temperature limit at which any particular ion could be studied. Product ions thermally decompose at temperatures where the primary ions are stable. A determination that thermal dissociation is occurring can usually only be made by varying the temperature. We have used the observation of thermal dissociation to get at processes that are otherwise difficult to determine. For instance, we have made determinations of the adiabatic electron affinities of hydrated electrons. Production of $Cl^-(CH_3Br)$ by ligand switching allowed one to study the dissociation of this ion for a well controlled energy distribution for the first time. This resulted in new insights into a reaction that had already been thoroughly studied. For $Cl^-(H_2O)_n$ and $F^-(H_2O)_n$ reacting with CH_3Br, we found that a H_2O ligand could be catalytically decomposed in a two-step process of ligand switching followed by thermal dissociation of the CH_3Br ligand.

One of the prime motivations for incorporating the supersonic ion source to the SIFT was to study reactions important for chemical ionization detection of trace neutrals. These studies have also proved interesting. The reactions of $CO_3^-(H_2O)_n$ ions with SO_2 showed that the rate constants varied substantially with cluster size and that one must be careful when using rate constants measured for a limited number of clusters. While the results of the study of $CO_3^-(H_2O)_n$ ions reacting with H_2SO_4 showed

no surprises, it was an important advance in that the study showed that any strongly bonded cluster ion (greater than about 10–12 kcal mol^{-1}) can be studied with most neutrals of interest. A particular challenge for atmospheric trace neutral detection will be the ability to study mixed clusters of the type $H^+(X)(H_2O)_n$ (where X are species such as acetone, acetonitrile or methanol) reacting with H_2O. The important question is whether the H_2O reactant can switch the X solvent molecule out of the cluster. This will have significant effects on the concentration of X derived from chemical ionization measurements. The SIFT with a supersonic ion source is an ideal apparatus to study these processes.

We have been able to show that measurements of rate constants with the source of the cluster ions in the flow tube often lead to erroneous results. The present method does not suffer from the fact that the ions are in equilibrium with the source gas. This effect has led to large errors in the past. Although some of the techniques described in the introduction can also get around this problem, they do not have the capability also to measure product distributions.

Our studies of hydration effects on nucleophilic displacement reactions have revealed new channels besides the expected channels. In particular, association and ligand switching were shown to replace nucleophilic displacement for larger cluster sizes. The versatility of the technique was demonstrated by showing that the Br^- signal coming from the reaction of $Cl^-(H_2O)$ with CH_3Br was not due to nucleophilic displacement but to ligand switching followed by thermal dissociation. Errors in previous measurements due to equilibrium in the flow tube appeared to be common in the nucleophilic displacement studies.

A completely unexpected aspect of the studies reviewed here is the indication that reactivity studies may reveal structural information about ions that cannot be derived from other measurements, that is whether ions are internally or externally solvated within a cluster. Our results seem to show that the switch from external to internal solvation occurs for larger hydration numbers as the size of the core ion increases. Also, it appears that polar reactant molecules may not be as good a probe of structural details as non-polar reactants because polar molecules can 'burrow' through the outer solvation layer. The results that we have found on this subject are intriguing but not definitive, and much more work needs to be done to validate this technique.

While many of the features of the studies presented here can be easily explained, there are several important unanswered questions that can benefit from theoretical studies and/or further experimental studies. The isotope effect in the reaction of $OH^-(H_2O)$ with CH_3Br is particularly intriguing. Although we have presented these results at numerous meetings and discussions, no satisfactory explanation of this isotope effect has arisen. The postulate that tunnelling is important in the thermal dissociation of $Cl^-(CH_3Br)$ is currently being examined. The difference in the temperature dependences of the fraction of Br^- produced in the reactions of $F^-(H_2O)$ and $OH^-(H_2O)$ with CH_3Br is puzzling as is the quantitative difference between the helium and H_2 buffers in the reaction of $OH^-(H_2O)_2$ with CH_3Br. Validation of the switch from external to internal solvation of ions is also important.

In conclusion, the addition of a supersonic ion source to a variable-temperature SIFT has resulted in numerous discoveries in the first years of use. Key to the success of this instrument is the use of a heated neutral inlet and the ability to vary the temperature. While the first studies have centred on negative-ion reactions, the instrument is equally capable of studying positive-ion reactions, and the first studies of positive ions are now under way.

Acknowledgements

We would like to thank all our collaborators on these projects too numerous to mention by name. In particular we would like to thank our engineers, John Williamson and Paul Mundis, for designing the modifications necessary to make these measurements. The Air Force Office of Scientific Research supported all this work under task 2303EP4, and the work on atmospheric ions was supported by SERDP. S. T. Arnold is under contract from the Aerodyne Research Corporation, Billerica, Massachusetts.

References

[1] Castleman, A. W., Jr, and Bowen, K. H., Jr, 1996, *J. phys. Chem.*, **100**, 12911.
[2] Graul, S. T., and Squires, R. R., 1988, *Mass Spectrom. Rev.* **7**, 263.
[3] Ferguson, E. E., Fehsenfeld, F. C., Dunkin, D. B., Schmeltekopf, A. L., and Schiff, H. I., 1964, *Planet. Space Sci.* **12**, 1169.
[4] Ferguson, E. E., Fehsenfeld, F. C., and Schmeltekopf, A. L., 1969, *Adv. at. molec. Phys.*, **5**, 1.
[5] Ferguson, E. E., and Fehsenfeld, F. C., 1968, *J. geophys. Res.*, **73**, 6215.
[6] Bohme, D. K., Dunkin, D. B., Fehsenfeld, F. C., and Ferguson, E. E., 1968, *J. chem. Phys.*, **49**, 5201.
[7] Bohme, D. K., Dunkin, D. B., Fehsenfeld, F. C., and Ferguson, E. E., 1969, *J. chem. Phys.*, **51**, 863.
[8] Ferguson, E. E., 1969, *Can. J. Chem.*, **47**, 1815.
[9] Fehsenfeld, F. C., Ferguson, E. E., and Bohme, D. K., 1969, *Planet. Space Sci.*, **17**, 1759.
[10] Ferguson, E. E., and Fehsenfeld, F. C., 1969, *J. geophys. Res., Space Phys.*, **74**, 5743.
[11] Fehsenfeld, F. C., and Ferguson, E. E., 1969, *J. geophys. Res.*, **74**, 2217.
[12] Fehsenfeld, F. C., Mosesman, M., and Ferguson, E. E., 1971, *J. chem. Phys.*, **55**, 2120.
[13] Howard, C. J., Rundle, H. W., and Kaufman, F., 1970, *J. chem. Phys.*, **53**, 3745.
[14] Howard, C. J., Rundle, H. W., and Kaufman, F., 1971, *J. chem. Phys.*, **55**, 4772.
[15] Howard, C. J., Rundle, H. W., and Kaufman, F., 1972, *J. chem. Phys.*, **57**, 3491.
[16] Bohme, D. K., 1984, *Ionic Processes in the Gas Phase*, edited by M. A. Almoster Ferreira (Boston, MA: Reidel) p. 111.
[17] Albritton, D. L., 1978, *At. Data nuc. Tables*, **22**, 1.
[18] Adams, N. G., and Smith, D., 1976, *Int. J. Mass Spectrom. Ion Phys.*, **21**, 349.
[19] Adams, N. G., and Smith, D., 1983, *Reactions of Small Transient Species*, edited by A. Fontijn and M. A. A. Clyne (New York: Academic Press) pp. 311–385.
[20] Smith, D., Adams, N. G., and Grief, D., 1977, *J. atmos. terr. Phys.*, **39**, 513.
[21] Smith, D., and Adams, N. G., 1978, *Chem. Phys. Lett.*, **54**, 535.
[22] Smith, D., and Adams, N. G., 1978, *Astrophys. J.*, **220**, L87.
[23] Smith, D., and Adams, N. G., 1988, *Adv. at. molec. Phys.*, **24**, 1.
[24] Smith, D., 1993, *Int. J. Mass Spectrom. Ion Phys.*, **129**, 1.
[25] Bates, D. R., 1984, *Chem. Phys. Lett.*, **112**, 41.
[26] Herbst, E., 1981, *J. chem. Phys.*, **75**, 4413.
[27] Viggiano, A. A., 1986, *J. chem. Phys.*, **84**, 244.
[28] Fahey, D. W., Bohringer, H., Fehsenfeld, F. C., and Ferguson, E. E., 1982, *J. chem. Phys.*, **76**, 1799.
[29] Bohringer, H., Fahey, D. W., Fehsenfeld, F. C., and Ferguson, E. E., 1983, *Planet. Space Sci.* **31**, 185.
[30] Viggiano, A. A., Deakyne, C. A., Dale, F., and Paulson, J. F., 1987, *J. chem. Phys.*, **87**, 6544.
[31] Rowe, B. R., Viggiano, A. A., Fehsenfeld, F. C., Fahey, D. W., and Ferguson, E. E., 1982, *J. chem. Phys.*, **75**, 742.
[32] Viggiano, A. A., Dale, F., and Paulson, J. F., 1988, *J. chem. Phys.*, **88**, 2469.
[33] Viggiano, A. A., Morris, R. A., Dale, F., and Paulson, J. F., 1988, *J. geophys. Res.*, **93**, 9534.
[34] Viggiano, A. A., and Arnold, F., 1995, *Atmospheric Electrodynamics*, edited by H. Volland (Boca Raton, LA: CRC Press) pp. 1–25.
[35] Yang, X., and Castleman, A. W., Jr, 1991, *J. Am. chem. Soc.*, **113**, 6766.

[36] YANG, X., and CASTLEMAN, A. W., JR, 1991, *J. phys. Chem.*, **95**, 6182.
[37] WINCEL, H., MEREAND, E., and CASTLEMAN, A. W. JR, 1996, *J. phys. Chem.*, **100**, 16808.
[38] HABERLAND, H., SCHINDLER, H. G., and WORSNOP, D. R., 1984, *Ber. Bunsenges. phys. Chem.*, **88**, 270.
[39] COE, J. C., SNODGRASS, J. T., FREIDHOFF, C. B., MCHUGH, K. M., and BOWEN, K. H., 1987, *J. chem. Phys.*, **87**, 4302.
[40] SEELEY, J. V., MORRIS, R. A., VIGGIANO, A. A., WANG, H., and HASE, W. L., 1997, *J. Am. chem. Soc.*, **119**, 577.
[41] VIGGIANO, A. A., MORRIS, R. A., DALE, F., PAULSON, J. F., GILES, K., SMITH, D., and SU, T., 1990, *J. chem. Phys.*, **93**, 1149.
[42] ARNOLD, S. T., MORRIS, R. A., and VIGGIANO, A. A., 1995, *J. chem. Phys.*, **103**, 9242.
[43] HABERLAND, H., LANGOSCH, H., SCHINDLER, H. G., and WORSNOP, D. R., 1984, *J. phys. Chem.*, **88**, 3903.
[44] KLOTS, C. E., 1985, *J. chem. Phys.*, **83**, 5854.
[45] BARNETT, R. N., LANDMAN, U., CLEVELAND, C. L., and JORTNER, J., 1988, *J. chem. Phys.*, **88**, 4429.
[46] BARNETT, R. N., LANDMAN, U., CLEVELAND, C. L., and JORTNER, J., 1988, *Chem. Phys. Lett.*, **145**, 382.
[47] CAMPAGNOLA, P. J., POSEY, L. A., and JOHNSON, M. A., 1991, *J. chem. Phys.*, **95**, 7998.
[48] CAMPAGNOLA, P. J., CYR, D. M., and JOHNSON, M. A., 1991, *Chem. Phys. Lett.*, **181**, 206.
[49] ARNOLD, S. T., MORRIS, R. A., VIGGIANO, A. A., and JOHNSON, M. A., 1996, *J. phys. Chem.*, **100**, 2900.
[50] POSEY, L. A., DELUCCA, M. J., CAMPAGNOLA, P. J., and JOHNSON, M. A., 1989, *J. phys. Chem.*, **93**, 1178.
[51] FERGUSON, E. E., 1983, *Chem. Phys. Lett.*, **99**, 89.
[52] VIGGIANO, A. A., 1993, *Mass Spectrum. Rev.*, **12**, 115.
[53] MIAKE-LYE, R. C., ANDERSON, B. E., COFER, W. F., WALLIO, H. A., NOWICKI, G. D., BALLENTHIN, J. O., HUNTON, D. E., KNIGHTON, W. B., MILLER, T. M., SEELEY, J. V., and VIGGIANO, A. A., 1998, *Geophys. Res. Lett.* (in the press).
[54] MÖHLER, O., and ARNOLD, F., 1992, *Geophys. Res. Lett.*, **17**, 1763.
[55] MÖHLER, O., and ARNOLD, F., 1991, *J. atmos. Chem.*, **13**, 33.
[56] MÖHLER, O., REINER, T., and ARNOLD, F., 1993, *Rev. scient. Instrum.*, **64**, 1199.
[57] HOFMANN, D. J., DESHLER, T., ARNOLD, F., and SCHLAGER, H., 1990, *Geophys. Res. Lett.*, **17**, 1279.
[58] ARNOLD, F., SCHEID, J., STILP, T., SCHLAGER, H., and REINHARDT, M. E., 1992, *Geophys. Res. Lett.*, **12**, 2421.
[59] SEELEY, J. V., MORRIS, R. A., and VIGGIANO, A. A., 1997, *Geophys. Res. Lett.*, **24**, 1379.
[60] VIGGIANO, A. A., SEELEY, J. V., MUNDIS, P. L., WILLIAMSON, J. S., and MORRIS, R. A., 1997, *J. phys. Chem.*, **101**, 8275.
[61] ALBRITTON, D. L., DOTAN, I., STREIT, G. E., FAHEY, D. W., FEHSENFELD, F. C., and FERGUSON, E. E., 1983, *J. chem. Phys.*, **78**, 6614.
[62] MÖHLER, O., REINER, T., and ARNOLD, F., 1992, *J. chem. Phys.*, **97**, 8233.
[63] LIAS, S. G., BARTMESS, J. E., LIEBMAN, J. F., HOLMES, J. L., LEVIN, R. D., and MALLARD, W. G., 1988, *J. phys. Chem. Ref. Data*, **17**, Suppl. 1, 1.
[64] CHASE, M. W., JR., DAVIES, C. A., DOWNEY, J. R., FRURIP, D. J., MCDONALD, R. A., and SYVERUD, A. N., 1985, *J. phys. Chem. Ref. Data*, **14**, Suppl. 1, 1.
[65] ARNOLD, S. T., MORRIS, R. A., and VIGGIANO, A. A., 1995, *J. chem. Phys.*, **103**, 2454.
[66] VIGGIANO, A. A., HENCHMAN, M. J., DALE, F., DEAKYNE, C. A., and PAULSON, J. F., 1992, *J. Am. chem. Soc.* **114**, 4299.
[67] IKEZOE, Y., MATSUOKA, S., TAKEBE, M., and VIGGIANO, A. A., 1987, *Gas Phase Ion–Molecule Reaction Rate Constants Through 1986* (Tokyo: Maruzen).
[68] VIGGIANO, A. A., ARNOLD, S. T., MORRIS, R. A., AHRENS, A. F., and HIERL, P. M., 1996, *J. phys. Chem.*, **100**, 14397.
[69] TANNER, D. J., and EISELE, F. L., 1995, *J. geophys. Res.*, **100**, 2883.
[70] BOHME, D. K., and MACKAY, G. I., 1981, *J. Am. chem. Soc.*, **103**, 978.
[71] HENCHMAN, M., PAULSON, J. F., and HIERL, P. M., 1983, *J. Am. chem. Soc.*, **105**, 5509.
[72] BOHME, D. K., and RAKSIT, A. B., 1984, *J. Am. chem. Soc.*, **106**, 3447.
[73] BOHME, D. K., and RAKSIT, A. B., 1985, *Can. J. Chem.*, **63**, 3007.

[74] Henchman, M., Hierl, P. M., and Paulson, J. F., 1985, *J. Am. chem. Soc.*, **107**, 2812.
[75] O'Hair, R. A. J., Davico, G. E., Hacaloglu, J., Dang, T. T., DePuy, C. H., and Bierbaum, V. M., 1994, *J. Am. chem. Soc.*, **116**, 3609.
[76] Morokuma, K. J., 1982, *J. Am. chem. Soc.*, **104**, 3732.
[77] Ohta, K., and Morokuma, K., 1985, *J. phys. Chem.*, **89**, 5845.
[78] Zhao, X. G., Lu, D., Liu, Y., Lynch, G. C., and Truhlar, D. G., 1992, *J. chem. Phys.*, **97**, 6369.
[79] Re, M., and Laria, D., 1996, *J. chem. Phys.*, **105**, 4584.
[80] Okuno, Y., 1996, *J. chem. Phys.*, **105**, 5817.
[81] Tanaka, K., Mackay, G. I., Payzant, J. D., and Bohme, D. K., 1976, *Can. J. Chem.*, **54**, 1643.
[82] Olmstead, W. N., and Brauman, J. I., 1977, *J. Am. chem. Soc.*, **99**, 4219.
[83] DePuy, C. H., Gronert, S., Mullin, A., and Bierbaum, V. M., 1990, *J. Am. chem. Soc.*, **112**, 8650.
[84] Hierl, P. M., Paulson, J. F., and Henchman, M. J., 1995, *J. phys. Chem.* **99**, 15655.
[85] Hierl, P. M., Ahrens, A. F., Henchman, M., Viggiano, A. A., Paulson, J. F., and Clary, D. C., 1986, *J. Am. chem. Soc.*, **108**, 3142.
[86] Su, T., Morris, R. A., Viggiano, A. A., and Paulson, J. F., 1990, *J. phys. Chem.*, **94**, 8426.
[87] Farneth, W. E., and Brauman, J. I., 1976, *J. Am. chem. Soc.*, **98**, 7891.
[88] Olmstead, W. P., 1977, Ph.D. Thesis, Stanford University.
[89] Brauman, J. I., 1979, *Kinetics of Ion–Molecule Reactions*, edited by P. Ausloos (New York: Plenum) pp. 153–164.
[90] Sen Sharma, D. K., and Kebarle, P., 1982, *J. Am. chem. Soc.*, **104**, 19.
[91] Magnera, T. F., and Kebarle, P., 1984, *Ionic Processes in the Gas Phase*, edited by M. A. Almoster Ferreira (Boston, MA: Reidel) pp. 135–157.
[92] Caldwell, G., Magnera, T. F., and Kebarle, P., 1984, *J. Am. chem. Soc.*, **106**, 959.
[93] Grimsrud, E. P., Chowdhury, S., and Kebarle, P., 1985, *J. chem. Phys.*, **83**, 1059.
[94] Sharma, R. B., Sen Sharma, D. K., Hiroaka, K., and Kebarle, P., 1985, *J. Am. chem. Soc.*, **107**, 3747.
[95] Meyer, S. A., 1987, Ph.D. Thesis, University of Kansas.
[96] Giles, K., and Grimsrud, E. P., 1992, *J. phys. Chem.*, **96**, 6680.
[97] Viggiano, A. A., 1984, *J. chem. Phys.*, **81**, 2639.
[98] Viggiano, A. A., Dale, F., and Paulson, J. F., 1985, *J. geophys. Res.*, **90**, 7977.
[99] Ferguson, E. E., 1986, *J. phys. Chem.*, **90**, 731.
[100] Viggiano, A. A., Morris, R. A., Paschkewitz, J. S., and Paulson, J. F., 1992, *J. Am. chem. Soc.*, **114**, 10477.
[101] Viggiano, A. A., Paschkewitz, J. S., Morris, R. A., Paulson, J. F., Gonzalez-Lafont, A., and Truhlar, D. G., 1991, *J. Am. chem. Soc.*, **113**, 9404.
[102] Knighton, W. B., Bognar, J. A., O'Conner, P. M., and Grimsrud, E. P., 1993, *J. Am. chem. Soc.*, **115**, 12079.
[103] Graul, S. T., and Bowers, M. T., 1991, *J. Am. chem. Soc.*, **113**, 9696.
[104] Cyr, D. M., Posey, L. A., Bishea, G. A., Han, C.-C., and Johnson, M. A., 1991, *J. Am. chem. Soc.*, **113**, 9697.
[105] Gronert, S., DePuy, C., and Bierbaum, V., 1991, *J. Am. chem. Soc.*, **113**, 4009.
[106] Ingemann, S., and Nibbering, N. M. M., 1984, *Can. J. Chem.*, **62**, 2273.
[107] Wang, H., Zhu, L., and Hase, W. L., 1994, *J. phys. Chem.*, **98**, 1608.
[108] Giles, K., and Grimsrud, E. P., 1993, *J. phys. Chem.*, **97**, 1318.
[109] Keesee, R. G., and Castleman, A. W. Jr, 1986, *J. phys. Chem. Ref. Data*, **15**, 1011.
[110] Graul, S. T., and Bowers, M. T., 1994, *J. Am. chem. Soc.*, **110**, 3875.
[111] Wang, H., and Hase, W. L., 1995, *J. Am. chem. Soc.*, **117**, 9347.
[112] Viggiano, A. A., and Morris, R. A., 1996, *J. phys. Chem.*, **100**, 19227.
[113] Seeley, J. V., Morris, R. A., and Viggiano, A. A., 1997, *J. phys. Chem.*, **101**, 4598.
[114] Hiraoka, K., Mizuse, S., and Yamabe, S., 1988, *J. phys. Chem.*, **92**, 3943.
[115] Xantheas, S. S., and Dunning, T. H., Jr, 1994, *J. phys. Chem.*, **98**, 13489.
[116] Xantheas, S. S., 1995, *J. Am. chem. Soc.*, **117**, 10373.
[117] Xantheas, S. S., and Dang, L. X., 1996, *J. phys. Chem.*, **100**, 3989.
[118] Glukhovtsev, M. N., Pross, A., and Radom, L., 1996, *J. Am. chem. Soc.*, **118**, 6273.

[119] Scott, A. P., and Radom, L., 1997, private communication.
[120] Combariza, J. E., Kestner, N. R., and Jortner, J., 1993, *Chem. Phys. Lett.*, **203**, 423.
[121] Combariza, J. E., and Kestner, N. R., 1994, *J. phys. Chem.*, **98**, 3513.
[122] Combariza, J. E., Kestner, N. R., and Jortner, J., 1994, *J. chem. Phys.*, **100**, 2851.
[123] Combariza, J. E., Kestner, N. R., and Jortner, J., 1994, *Chem. Phys. Lett.*, **221**, 156.
[124] Perera, L., and Berkowitz, M. L., 1993, *J. chem. Phys.*, **99**, 4222.
[125] Perera, L., and Berkowitz, M. L., 1994, *J. chem. Phys.*, **100**, 3085.
[126] Asada, T., Nishimoto, K., and Kitaura, K., 1993, *J. phys. Chem.*, **97**, 7724.
[127] Dang, L. X., and Garret, B. C., 1993, *J. chem. Phys.*, **99**, 2972.
[128] Jorgensen, W. L., and Severance, D. L., 1993, *J. chem. Phys.*, **99**, 4233.
[129] Sremaniak, L. S., Perera, L., and Berkowitz, M. L., 1996, *J. phys. Chem.*, **100**, 1350.
[130] Cheshnovsky, O., Giniger, R., Markovich, G., Makov, G., Nitzan, A., and Jortner, J., 1995, *J. Chim. phys.*, **92**, 397.
[131] Arshadi, M., Yamdagni, R., and Kebarle, P., 1970, *J. phys. Chem.*, **74**, 1475.
[132] Keesee, R. G., Castleman, A. W. J. 1980, *Chem. Phys. Lett.*, **74**, 139.
[133] Markovich, G., Pollack, S., Giniger, R., Cheshnovsky, O., 1993, *Z. Phys.* D, **26**, 98.
[134] Markovich, G., Pollack, S., Giniger, R., and Cheshnovsky, O., 1994, *J. chem. Phys.*, **101**, 9344.
[135] Seeley, J. V., Morris, R. A., and Viggiano, A. A., 1996, *J. phys. Chem.*, **100**, 15821.
[136] Arnold, S. T., and Viggiano, A. A., 1997, *J. phys. Chem.*, **101**, 2859.